March 2021

Accelerated Gradient Descent Methods For the Uniaxially Constrained Landau-de Gennes Model

Edison E. Chukwuemeka
Louisiana State University and Agricultural and Mechanical College

Accelerated Gradient Descent Methods For the Uniaxially Constrained Landau-de Gennes Model

A Masters Thesis

Submitted to the Graduate Faculty of the
Louisiana State University and
Agricultural and Mechanical College
in partial fulfillment of the
requirements for the degree of
Master of Science

in

Department of Mathematics

by
Edison Ekperechukwu Chukwuemeka
B.Sc., Univerisity of Lagos, 2008
May, 2021

Dedication

Dedicated to my parents

Acknowledgments

Gratitude and appreciation goes to my family, Olawunmi and Edison Jr, my parents and siblings. I am eternally indebted to them for their support, love and prayers in the course of the program.

I would like to give my deepest gratitude to my supervisor, Dr. Shawn Walker, whose knowledge of numerical computation has been vital in completing this project. Discussions with him on the implementation of the minimization scheme using a MATLAB toolbox he developed has further refined my understanding of implementing the minimization schemes.

I also thank my committee members, Dr. Blaise Bourdin and Dr. Ingmar Schoegl for accepting to serve as a member of the committee.

Finally and above all, I give thanks to God Almighty for his providence and sustenance during the program.

The numerical computations in this Thesis were implemented using the MATLAB/C++ toolbox - FELICITY.

Table of Contents

List of Tables

List of Figures

Abstract

Liquid crystal models with the capability of capturing defects has been one of the main focus in modeling the behavior of such phase mathematically. A uni-axially constrained Landau-de Gennes one-constant model, which has this capability was modeled using three minimization schemes - standard gradient descent, Nesterov accelerated gradient descent, and heavy-ball accelerated gradient descent. The uni-axially constrained Landau-de Gennes energy is discretized using finite element method and the performance of the minimization schemes are measured using the classical gradient descent scheme as the baseline. The numerical experiments conducted indicated that the accelerated gradient descent schemes improved the convergence rate and reduced the duration of the computation while maintaining the same minimum energy.

Chapter 1.
Introduction

1.1. Liquid Crystals

Liquid crystals (LC) discovered in 1888 by F. Reinitzer and O. Lehmann are intermediate state of matters which possess the characteristics of both liquids and solids depending on the condition imposed on it. These mesogenic materials possess some of degree of orientation and positional order depending on the imposed condition on materials [1]. The micro-structure of liquid crystals can be manipulated via mechanical, chemical, optical and thermal properties of the material.

Liquid crystals (LCs) are important in many emerging technologies [2, 3]. They are easily actuated by optical effects [4–8], electric/magnetic [9–11], and mechanical forces [12–15], which has yielded various devices, e.g. electronic shutters [16], novel types of lasers [17, 18], dynamic shape control of elastic bodies [19, 20], and others [21–25].

These mesophases are formed by either purely thermal processes or by the influence of the concentration of the solvents. The liquid crystals formed by the thermal excitation are called thermotropics while those formed as a result of the concentration of the solvents are called lyotropics.

1.2. Classification of Liquid Crystals

Liquid crystals are classified as follows:

- Nematic Liquid Crystals: The molecules of this mesophase are mostly oriented or aligned in a preferred direction. This mesophase is characterized by the long-range orientation order [26, 27]. The local orientation of the molecules is defined by the vector $\mathbf{n}(\mathbf{r})$ usually called the director.

- Cholesteric Liquid Crystals: These class of liquid crystals are similar to the nematic liquid crystal in terms of the long-range orientation order. However, the director of the molecules varies in the form of an helix. In the absence of external excitation, the orientation of the

cholesteric liquid crystals could be given as follows in the cartesian coordinates [1]:

$$\mathbf{n} = (cos(\tau z + \varphi_0), sin(\tau z + \varphi_0), 0) \tag{1.1.}$$

τ is a scalar called twist, $\varphi_0 \in [0, 2\pi]$ is an angle.

Other liquid crystals are Smectics and the columnar phases.

1.3. Modeling of Nematic Liquid Crystals

The mathematical modeling of LCs is quite exhaustive that many researchers have proposed different ways to model this mesophase. This section gives a brief summary of the different theories used to model LCs. These are the Frank-Oseen theory, Ericksen-Leslie theory, and Landau-de Gennes theory etc.

1.3.1. Oseen-Frank Model

Suppose the mean molecular alignment at a location $\mathbf{x}$ in a given volume Ω of the nematic LC is described by a vector $\mathbf{n}$ called the director such that:

$$\mathbf{n} = \mathbf{n}(\mathbf{x}), \qquad \mathbf{n} \cdot \mathbf{n} = 1 \tag{1.2.}$$

The total elastic energy of the nematic LC is defined as [28]:

$$\mathrm{E_{OF}} = \int_{\Omega} w(\mathbf{n}, \nabla \mathbf{n}) d\Omega \tag{1.3.}$$

The free energy $w(\mathbf{n}, \nabla \mathbf{n})$ satisfies the following the properties:

- Positive Definiteness: In the absence of any external conditions imposed on the LC, it relax to the natural orientation, which is the undistorted state of the molecules. Thus the elastic energy of the molecules is zero. However, in the presence of an external condition which disturbs the natural orientation of the molecules, energy is expended to minimize the elastic

energy attained at equilibrium. This results in a positive elastic energy of the LC.

$$w(\mathbf{n}, \nabla\mathbf{n}) \geq 0 \tag{1.4.}$$

- Eveness:

$$w(-\mathbf{n}, -\nabla\mathbf{n}) = w(\mathbf{n}, \nabla\mathbf{n}) \tag{1.5.}$$

- Frame Indifference:

$$w(\mathbf{n}, \nabla\mathbf{n}) = w(\mathbf{Q}\mathbf{n}, \mathbf{Q}\nabla\mathbf{n}\mathbf{Q}^{\mathrm{T}}) \tag{1.6.}$$

$\mathbf{Q}$ is any orthogonal matrix whose $det(\mathbf{Q}) = 1$ and $\mathbf{Q}^{\mathrm{T}}$ is the transpose of the orthogonal matrix.

The free energy $w(\mathbf{n}, \nabla\mathbf{n})$ of the nematic LC is given as:

$$\begin{aligned} w(\mathbf{n}, \nabla\mathbf{n}) = \frac{1}{2}\Big[\mathrm{K}_1 (\nabla \cdot \mathbf{n})^2 + \mathrm{K}_2 (\mathbf{n} \cdot \nabla \times \mathbf{n})^2 + \mathrm{K}_3 (\mathbf{n} \times \nabla \times \mathbf{n})^2\Big] \\ + \frac{1}{2}\left[(\mathrm{K}_2 + \mathrm{K}_4)\nabla \cdot [(\mathbf{n} \cdot \nabla)\mathbf{n} - (\nabla \cdot \mathbf{n})\mathbf{n}]\right] \end{aligned} \tag{1.7.}$$

K_i are known as the Frank's constant. $\mathrm{K}_1, \mathrm{K}_2, \mathrm{K}_3$ are called splay, twist, and bend constants respectively, while $(\mathrm{K}_2 + \mathrm{K}_4)$ is called the saddle splay constant.

Assuming $\mathrm{K}_1 = \mathrm{K}_2 = \mathrm{K}_3 = \kappa$, and $\mathrm{K}_4 = 0$, the free energy reduces to the one constant approximation as follows:

$$w(\mathbf{n}, \nabla\mathbf{n}) = \frac{\kappa}{2}\|\nabla\mathbf{n}\|^2 \tag{1.8.}$$

The Oseen-Frank one constant approximation is given as:

$$\mathrm{E}_{\mathrm{OF}} = \frac{\kappa}{2}\int_{\Omega} \|\nabla\mathbf{n}\|^2 d\Omega \tag{1.9.}$$

1.3.2. Landau-deGennes Model

The limitation of Oseen-Frank model is that it could not capture defects which are common in materials. However, the Landau-deGennes model uses a second-order tensor $\mathbf{Q}$ - the order parameter to model the energy of the liquid crystal. This model was able to capture defects in materials. The bulk energy of the liquid crystal model is defined as [2, 26]:

$$\mathrm{E}_{\mathrm{LDF,B}ulk} = \mathrm{F}_0 + \frac{1}{2}\mathrm{A}(\mathrm{T})\sum_{\rho,\alpha}\mathbf{Q}_{\alpha,\beta}\mathbf{Q}_{\alpha\beta} + \frac{1}{3}\mathrm{B}(\mathrm{T})\sum_{\alpha,\beta,\gamma}\mathbf{Q}_{\alpha\beta}\mathbf{Q}_{\alpha\gamma}\mathbf{Q}_{\gamma\alpha} + \mathrm{O}(\mathbf{Q}^4) \tag{1.10.}$$

F_0 is a constant, $\mathrm{A}(\mathrm{T})$ and $\mathrm{B}(\mathrm{T})$ are temperature dependent coefficients. The elastic energy part of the LC model is defined as

$$\mathrm{E}_{\mathrm{LDG,E}l} = \frac{1}{2}\int_{\Omega}|\nabla\mathbf{Q}|^2 d\mathbf{x} \tag{1.11.}$$

1.3.3. Ericksen Model

This theory introduced an additional term called the degree of orientation s to describe the state of the nematic LC. To accomplish this theory, the order tensor $\mathbf{Q}$ for uniaxial nematics are defined in terms of s and $\mathbf{n}$ as [1, 28, 29]:

$$\mathbf{Q} = s(\mathbf{n}\otimes\mathbf{n} - \frac{1}{3}\mathbf{I}) \tag{1.12.}$$

$\mathbf{I}$ is the identity tensor, $s \in [-\frac{1}{2}, 1]$.

The energy functional of the nematic LC occupying a region Ω in space is given as:

$$\mathrm{E}_{\mathrm{E}rk}[s,\mathbf{n}] := \int_{\Omega} w_{\mathrm{E}rk}(s,\nabla s,\mathbf{n},\nabla\mathbf{n})d\Omega \tag{1.13.}$$

$$\begin{aligned} w_{\mathrm{E}rk}(s,\nabla s,\mathbf{n},\nabla\mathbf{n}) &= k_1(\nabla\cdot\mathbf{n})^2 + k_2(\mathbf{n}\cdot[\nabla\times\mathbf{n}])^2 + k_3|\mathbf{n}\times(\nabla\times\mathbf{n})|^2 \\ &+(k_2+k_4)(\mathrm{tr}(\nabla\mathbf{n})^2 - (\mathrm{div}\,\mathbf{n})^2) + k_5|\nabla s - (\nabla s\cdot\mathbf{n})\mathbf{n} - \lambda(\nabla\mathbf{n})\mathbf{n}|^2 \\ &+k_6(\nabla s\cdot\mathbf{n} - \mu\mathrm{div}\,\mathbf{n})^2 + \psi(s) \end{aligned} \tag{1.14.}$$

$\psi(s) = \frac{1}{2}as^2 - \frac{1}{3}bs^3 + \frac{1}{4}cs^4 + d$ is the potential.

The one constant approximation of the Ericksen-Leslie model is given as:

$$\mathrm{E}_{erk} = \int_\Omega \left(\kappa|\nabla s|^2 + s^2|\nabla \mathbf{n}|^2\right) d\Omega + \int_\Omega \psi(s) d\Omega \tag{1.15.}$$

such that $\kappa > 0$ and $s \in [-\frac{1}{2}, 1]$.

1.4. Research Objectives

LC models use an order parameter that represents the statistical average of the orientation of the LC molecules [1]. The Landau-de Gennes (LdG) model is popular and uses a *tensor-valued* function $\mathbf{Q}$ to model the orientational state of the LC material. In particular, the eigenframe of $\mathbf{Q}$ yields information about the distribution of LC molecules. Moreover, the energy functional (of $\mathbf{Q}$) for the LC material involves an elastic contribution and a bulk potential. Equilibrium LC states are minimizers of the energy functional.

This thesis is concerned with a specific variant of the LdG model where *uniaxiality* is enforced as a hard constraint (see section 2.1.). This leads to a "non-smooth" energy that is difficult to minimize. Standard gradient descent methods are robust, but can be extremely slow to converge to a minimizer. Therefore, we investigate alternative methods for minimizing the energy functional, so-called accelerated gradient descent methods, e.g. the "heavy-ball" method and Nesterov's method. Our numerical experiments clearly show that the heavy-ball method is vastly superior to standard gradient descent, even in the presence of the *non-smoothness* of the model; we also show that Nesterov's method is an improvement as well. Although many numerical methods and implementations exist for the standard LdG model, e.g. [30–36], to the best of our knowledge, accelerated gradient methods for LC simulations are not typically used.

This thesis is organized as follows. A review of the Landau-de Gennes model using the one constant approximation is presented in chapter 2.. The formulation of the minimization method of the Landau-de Gennes energy is described then the accelerated gradient approach is presented alongside with the algorithm used to implement the finite element solution.

Chapter 3. gives the the numerical experiments conducted with the described algorithms on computing the point defects of a liquid crystal domain. A comparison of the methods is presented to determine the optimized method that minimize the uniaxially constrained Landau-de Gennes energy of nematic liquid crystals.

Chapter 4. concludes the thesis with the outcome of the numerical experiments conducted.

Chapter 2.
The Landau-de Gennes Model

Considering the Landau-de Gennes model [2, 37], let $\Omega \subset \mathbb{R}^d$, with $d = 2, 3$, be the domain of the LC material (assume Ω is Lipschitz). The order parameter $\mathbf{Q}$ is a tensor-valued function $\mathbf{Q} : \Omega \to \mathbf{\Lambda}$, where

$$\mathbf{\Lambda} := \{\mathbf{A} \in \mathbb{R}^{d\times d} \mid \mathbf{A} = \mathbf{A}^{\mathrm{T}},\ \mathrm{tr}(\mathbf{A}) = 0\}. \tag{2.1.}$$

The "one-constant" energy functional for $\mathbf{Q}$ is

$$\mathrm{E}_{\mathrm{LdG}}[\mathbf{Q}] := \frac{1}{2}\int_\Omega |\nabla \mathbf{Q}|^2\, d\mathbf{x} + \frac{1}{\epsilon_{\mathrm{dw}}^2}\int_\Omega \psi_{\mathrm{LdG}}(\mathbf{Q})\, d\mathbf{x}, \tag{2.2.}$$

where $\epsilon_{\mathrm{dw}} > 0$ is a material parameter (nematic correlation length-scale), and ψ_{LdG} is a "bulk" (thermotropic) potential. Note: $|\nabla \mathbf{Q}|^2 = \sum_{i,j,k}(\partial_k \mathrm{Q}_{ij})^2$. More complicated models can also be considered [2, 37, 38].

The bulk potential ψ_{LdG} is a double-well type of function that captures the nematic to isotropic phase transition of nematic LCs. Mathematically, it tries to confine the eigenvalues of $\mathbf{Q}$ to the physically meaningful range $\lambda_i \in [-1/d, 1-1/d]$, where the simplest form is given by

$$\psi_{\mathrm{LdG}}(\mathbf{Q}) = \mathrm{K} + \frac{\mathrm{A}}{2}\mathrm{tr}(\mathbf{Q}^2) - \frac{\mathrm{B}}{3}\mathrm{tr}(\mathbf{Q}^3) + \frac{\mathrm{C}}{4}\Big(\mathrm{tr}(\mathbf{Q}^2)\Big)^2. \tag{2.3.}$$

Above, A, B, C are material parameters such that A may be positive or negative, and B, C are positive; K is a convenient constant. Critical points of ψ_{LdG} are either isotropic or uniaxial $\mathbf{Q}$-tensors [39]; moreover, we let $\mathrm{A} \le 0$ in order to favor uniaxial states over isotropic states, so we assume that

$$\mathrm{A} \le 0, \quad \mathrm{B}, \mathrm{C} > 0, \tag{2.4.}$$

which implies that $\psi_{\mathrm{LdG}}(\mathbf{Q}) \ge 0$ assuming K is suitably chosen. In two dimensions, $\mathrm{tr}(\mathbf{Q}^3) = 0$,

because $\mathbf{Q}^2 = \frac{s^2}{4}\mathbf{I}$. Hence, B is irrelevant when $d = 2$.

One seeks to minimize (2.2.) over $\mathbf{Q}$ in $\mathrm{H}^1(\Omega;\mathbf{\Lambda})$ with suitable boundary conditions, e.g. Dirichlet. When $d = 3$, a simple argument [37] shows that minimizers of $\mathbf{Q} \mapsto \int_\Omega \psi_{\mathrm{LdG}}(\mathbf{Q})$ have a uniaxial form, i.e.

$$\mathbf{Q} = s\Big(\mathbf{n}\otimes\mathbf{n} - \frac{1}{3}\mathbf{I}\Big), \tag{2.5.}$$

where $\mathbf{n} \in \mathbb{S}^2$ and $s \in [-1/2, 1]$. However, general minimizers of (2.2.) are not necessarily uniaxial; they are typically *biaxial* [40–42]:

$$\mathbf{Q} = -s_1\Big(\mathbf{n}_1\otimes\mathbf{n}_1 - \frac{1}{3}\mathbf{I}\Big) - s_2\Big(\mathbf{n}_2\otimes\mathbf{n}_2 - \frac{1}{3}\mathbf{I}\Big) \tag{2.6.}$$

where $\mathbf{n}_1, \mathbf{n}_2 \in \mathbb{S}^2$, $\mathbf{n}_1\cdot\mathbf{n}_2 = 0$, and $s_1 = -2\lambda_1 - \lambda_2$, $s_2 = -\lambda_1 - 2\lambda_2$. Note: when $d = 2$, $\mathbf{Q}$ always has the form $\mathbf{Q} = s\big(\mathbf{n}\otimes\mathbf{n} - \frac{1}{2}\mathbf{I}\big)$.

But this brings up a modeling issue. Some types of LCs do exhibit biaxiality [43], such as lyotropic LCs (see [44]). But thermotropic LCs do not typically exhibit a biaxial phase in experiments; Indeed, a biaxial phase was only first reported in [45–47]. Therefore, it is plausible that uniaxiality should be an *inherent* part of the model for some types of LC systems. Here, we consider the LdG model with uniaxiality enforced as a *hard constraint* (see Section 2.1.). The main contribution here is to illustrate alternative minimization schemes to compute energy minimizers with such a *non-smooth constraint* (see Section 2.2.).

2.1. The Uniaxially Constrained Q-Model

This section describes the mathematical formulation of the minimization problem for the one-constant Landau-deGennes energy $\mathrm{E}_{\mathrm{LdG}}$ under the uniaxiality constraint (2.5.) (Section 2.1.1.). The model we obtain has similarities with the Ericksen model [34, 48–50], but it has the advantage of allowing for non-orientable minimizers that exhibit half-integer order defects. This model is mainly of interest when $d = 3$, since when $d = 2$, $\mathbf{Q}$ necessarily has the form of a uniaxial tensor. A small advantage of this approach is that it yields a model with fewer variables; the standard LdG model involves a non-linear system with five coupled variables in 3-D [32, 35, 36, 51].

In addition, the uniaxial model provides a way to easily control the eigenvalues of $\mathbf{Q}$, which the standard model does not. For more information on the uniaxial model and discretization (Section 2.1.2.), see [34].

Remark 1 *Uniaxial models arise in a small elastic constant limit. In [52], the one-constant model* (2.2.) *is studied with a small bulk coefficient* ϵ_{dw} *(which is equivalent to a small elastic constant). Under suitable boundary conditions, in the limit* $\epsilon_{\mathrm{dw}} \to 0$*, Landau-de Gennes minimizers converge to minimizers of the Oseen-Frank energy. The analysis in [52] is refined in [53], where the dependence of the difference between the solution to both models with respect to* ϵ_{dw} *is analyzed.*

2.1.1. Theoretical Background

For a uniaxially constrained $\mathbf{Q}$-tensor as in (2.5.), set $\mathbf{\Theta} = \mathbf{n} \otimes \mathbf{n}$ and minimize (2.2.) with respect to s and $\mathbf{\Theta}$. Define the space

$$\mathrm{L}^{d-1} = \{\mathbf{A} \in \mathbb{R}^{d\times d} : \text{there exists } \mathbf{n} \in \mathbb{S}^{d-1},\ \mathbf{A} = \mathbf{n}\otimes\mathbf{n}\}, \tag{2.7.}$$

which is isomorphic to the real projective space $\mathbf{RP}^{d-1}$ by the map $\mathbf{n}\otimes\mathbf{n} \longmapsto \{\mathbf{n}, -\mathbf{n}\}$. So the uniaxially constrained LdG model accounts for the molecular *direction* (i.e. a line segment) but not the orientation (i.e. a vector).

Since $\nabla\mathbf{Q} = \nabla s \otimes \left(\mathbf{\Theta} - \frac{1}{d}\mathbf{I}\right) + s\nabla\mathbf{\Theta}$, we get

$$|\nabla\mathbf{Q}|^2 = |\nabla s|^2 \left|\mathbf{\Theta} - \frac{1}{d}\mathbf{I}\right|^2 + s^2|\nabla\mathbf{\Theta}|^2 + 2s\left[\nabla s \otimes \left(\mathbf{\Theta} - \frac{1}{d}\mathbf{I}\right)\right] : \nabla\mathbf{\Theta}.$$

A simple calculation gives $\left|\mathbf{\Theta} - \frac{1}{d}\mathbf{I}\right|^2 = \frac{d-1}{d}$ and $\left[\nabla s \otimes \left(\mathbf{\Theta} - \frac{1}{d}\mathbf{I}\right)\right] : \nabla\mathbf{\Theta} = 0$, so that

$$|\nabla\mathbf{Q}|^2 = \frac{d-1}{d}|\nabla s|^2 + s^2|\nabla\mathbf{\Theta}|^2. \tag{2.8.}$$

Note the following straightforward equalities:

$$\begin{aligned}&\text{for } d=2: \quad (1/2)s^2=\mathrm{tr}(\mathbf{Q}^2), \quad 0=\mathrm{tr}(\mathbf{Q}^3), \quad (1/4)s^4=(\mathrm{tr}(\mathbf{Q}^2))^2,\\ &\text{for } d=3: \quad (2/3)s^2=\mathrm{tr}(\mathbf{Q}^2), \quad (2/9)s^3=\mathrm{tr}(\mathbf{Q}^3), \quad (4/9)s^4=(\mathrm{tr}(\mathbf{Q}^2))^2.\end{aligned} \tag{2.9.}$$

Therefore, the one-constant energy for the uniaxially constrained $\mathbf{Q}$-tensor model is obtained by plugging (2.8.) into (2.2.) to get

$$\begin{aligned}&\mathrm{E}_{\mathrm{LdG}}[\mathbf{Q}]=\mathrm{E}_{\mathrm{uni}}[s,\boldsymbol{\Theta}]:=\mathrm{E}_{\mathrm{uni-m}}[s,\boldsymbol{\Theta}]+\mathrm{E}_{\mathrm{LdG,bulk}}[s],\\ &\mathrm{E}_{\mathrm{uni-m}}[s,\boldsymbol{\Theta}]:=\frac{1}{2}\left(\frac{d-1}{d}\int_\Omega|\nabla s|^2\,dx+\mathring{\mathrm{E}}_{\mathrm{uni}}[s,\boldsymbol{\Theta}]\right),\\ &\mathring{\mathrm{E}}_{\mathrm{uni}}[s,\boldsymbol{\Theta}]:=\int_\Omega s^2|\nabla\boldsymbol{\Theta}|^2\,dx, \qquad \mathrm{E}_{\mathrm{LdG,bulk}}[s]:=\frac{1}{\epsilon_{\mathrm{dw}}^2}\int_\Omega\psi_{\mathrm{LdG}}(s)\,dx,\end{aligned} \tag{2.10.}$$

where, with some abuse of notation, we write $\psi_{\mathrm{LdG}}(s):=\psi_{\mathrm{LdG}}(\mathbf{Q})$. The admissible class for minimization becomes more clear upon using the following change of variable $\mathbf{U}=s\boldsymbol{\Theta}$ and rewrite

$$\mathrm{E}_{\mathrm{uni-m}}[s,\boldsymbol{\Theta}]=\widetilde{\mathrm{E}}_{\mathrm{uni-m}}[s,\mathbf{U}]:=\frac{1}{2}\left(-\frac{1}{d}\int_\Omega|\nabla s|^2\,dx+\int_\Omega|\nabla\mathbf{U}|^2\,dx\right). \tag{2.11.}$$

Since the degree of orientation s needs to satisfy $s\in[-\frac{1}{d-1},1]$, we define the admissible class as

$$\mathcal{A}_{\mathrm{uni}}:=\{(s,\boldsymbol{\Theta})\in\mathrm{H}^1(\Omega)\times[\mathrm{L}^\infty(\Omega)]^{d\times d}:(s,\mathbf{U},\boldsymbol{\Theta}) \text{ satisfies (2.13.), with } \mathbf{U}\in[\mathrm{H}^1(\Omega)]^d\}, \tag{2.12.}$$

with the structural condition

$$-\frac{1}{d-1}\le s\le 1, \qquad \mathbf{U}=s\boldsymbol{\Theta}, \qquad \boldsymbol{\Theta}\in\mathrm{L}^{d-1} \text{ a.e. in } \Omega. \tag{2.13.}$$

In order to enforce boundary conditions on $(s,\boldsymbol{\Theta})$, on different parts of the boundary, we introduce auxiliary functions $g:\Omega\to(-\frac{1}{d-1},1)$ and $\mathbf{M}:\Omega\to\mathrm{L}^{d-1}$ and define the restricted

admissible class

$$\mathcal{A}_{\text{uni}}(g,\mathbf{M}) := \left\{(s,\boldsymbol{\Theta}) \in \mathcal{A}_{\text{uni}} :\ s|_{\Gamma_s} = g, \quad \boldsymbol{\Theta}|_{\Gamma_{\boldsymbol{\Theta}}} = \mathbf{M}\right\}, \tag{2.14.}$$

where Γ_s and $\Gamma_{\boldsymbol{\Theta}}$ are open subsets of $\partial\Omega$ on which to enforce Dirichlet conditions for s and $\boldsymbol{\Theta}$ (respectively).

See [34] for more details on the function spaces and theoretical details. In this thesis, we are only concerned with the minimization scheme for the discrete problem (Section 2.2.).

2.1.2. Discretization

We discretize $\Omega \subset \mathbb{R}^d$ with a conforming simplicial shape-regular triangulation $\mathcal{T}_h = \{\mathrm{T}_i\}$ (ignoring any geometric error caused by domain approximation), with nodes (vertices) $\mathcal{N}_h$. Moreover, we assume the mesh is weakly-acute, which is necessary because of the form of our discrete energy.

Next, define continuous linear Lagrange finite element spaces on Ω, i.e. let s_h in $\mathbb{S}_h$, and $\boldsymbol{\Theta}_h$ in $\mathbb{T}_h$, be the finite element approximations of s and $\boldsymbol{\Theta}$, where

$$\begin{aligned}
\mathbb{S}_h &:= \{z_h \in \mathrm{H}^1(\Omega) : z_h|_{\mathrm{T}} \in \mathcal{P}_1(\mathrm{T}), \forall \mathrm{T} \in \mathcal{T}_h\}, \\
\overline{\mathbb{U}}_h &:= \{\mathbf{U}_h \in [\mathrm{H}^1(\Omega)]^{d\times d} : \mathbf{U}_h|_{\mathrm{T}} \in \mathcal{P}_1(\mathrm{T}), \forall \mathrm{T} \in \mathcal{T}_h\}, \\
\mathbb{T}_h &:= \{\boldsymbol{\Theta}_h \in \overline{\mathbb{U}}_h : \boldsymbol{\Theta}_h(x_i) \in \mathrm{L}^{d-1}, \forall x_i \in \mathcal{N}_h\},
\end{aligned} \tag{2.15.}$$

where $\mathbb{T}_h$ imposes the rank-one, unit norm constraint only at the vertices of the mesh. Dirichlet boundary conditions are included via the following discrete spaces:

$$\mathbb{S}_h(\Gamma_s, g_h) := \{s_h \in \mathbb{S}_h : s_h|_{\Gamma_s} = g_h\}, \quad \mathbb{T}_h(\Gamma_{\boldsymbol{\Theta}}, \mathbf{M}_h) := \{\boldsymbol{\Theta}_h \in \mathbb{T}_h : \boldsymbol{\Theta}_h|_{\Gamma_{\boldsymbol{\Theta}}} = \mathbf{M}_h\},$$

where $g_h := \mathrm{I}_h g$ and $\mathbf{M}_h := \mathrm{I}_h \mathbf{M}$ are the discrete Dirichlet data. This yields the discrete admis-

sible class with boundary conditions:

$$\mathcal{A}^h_{\text{uni}}(g_h, \mathbf{M}_h) := \Big\{(s_h, \boldsymbol{\Theta}_h) \in \mathbb{S}_h(\Gamma_s, g_h) \times \mathbb{T}_h(\Gamma_{\boldsymbol{\Theta}}, \mathbf{M}_h) : (s_h, \mathbf{U}_h, \boldsymbol{\Theta}_n) \text{ satisfies (2.17.)}\Big\}, \quad (2.16.)$$

where

$$\mathbf{U}_h = \mathrm{I}_h(s_h\boldsymbol{\Theta}_h) \in \overline{\mathbb{U}}_h, \quad -\frac{1}{d-1} \le s_h \le 1 \text{ in } \Omega, \quad \text{and } \boldsymbol{\Theta}_h(x_i) \in \mathrm{L}^{d-1},\ \forall x_i \in \mathcal{N}_h, \qquad (2.17.)$$

is called the *discrete structural condition* of $\mathcal{A}^h_{\text{uni}}$.

The discrete version of $\mathrm{E}_{\text{uni-m}}[s, \boldsymbol{\Theta}]$ is derived in [34]. We set $\delta_{ij}s_h := s_h(x_i) - s_h(x_j)$, and $\delta_{ij}\boldsymbol{\Theta}_h := \boldsymbol{\Theta}_h(x_i) - \boldsymbol{\Theta}_h(x_j)$, for $x_i, x_j \in \mathcal{N}_h$, and define the main part of the discrete energy to be

$$\mathrm{E}^h_{\text{uni-m}}[s_h, \boldsymbol{\Theta}_h] := \frac{d-1}{4d} \sum_{i,j=1}^{n} k_{ij}\Big(\delta_{ij}s_h\Big)^2 + \frac{1}{4}\sum_{i,j=1}^{n} k_{ij}\left(\frac{s_h(x_i)^2 + s_h(x_j)^2}{2}\right)|\delta_{ij}\boldsymbol{\Theta}_h|^2. \qquad (2.18.)$$

The first term corresponds to

$$\frac{1}{2}\sum_{i,j=1}^{n} k_{ij}\Big(\delta_{ij}s_h\Big)^2 = \int_\Omega |\nabla s_h|^2 dx,$$

while the second term is a first order approximation of $\frac{1}{2}\int_\Omega s^2|\nabla\boldsymbol{\Theta}|^2 dx$. For convenience, we shall denote

$$\mathring{\mathrm{E}}^h_{\text{uni}}[s_h, \boldsymbol{\Theta}_h] := \frac{1}{2}\sum_{i,j=1}^{n} k_{ij}\left(\frac{s_h(x_i)^2 + s_h(x_j)^2}{2}\right)|\delta_{ij}\boldsymbol{\Theta}_h|^2. \qquad (2.19.)$$

The bulk energy is discretized in the same way as before,

$$\mathrm{E}^h_{\text{LdG,bulk}}[s_h] := \frac{1}{\epsilon^2_{\text{dw}}}\int_\Omega \psi_{\text{LdG}}(s_h) dx. \qquad (2.20.)$$

With the notation introduced above, the formulation of the discrete problem reads as follows.

Find $(s_h, \Theta_h) \in \mathbb{S}_h(\Gamma_s, g_h) \times \mathbb{T}_h(\Gamma_\Theta, \mathrm{M}_h)$ such that the following energy is minimized:

$$\mathrm{E}^h_{\mathrm{uni}}[s_h, \Theta_h] := \mathrm{E}^h_{\mathrm{uni-m}}[s_h, \Theta_h] + \mathrm{E}^h_{\mathrm{LdG,bulk}}[s_h]. \tag{2.21.}$$

The Γ-convergence of this discrete energy was shown in [34].

2.2. Review of Gradient Based Minimization Schemes

We give a general discussion of gradient descent and *accelerated* gradient descent methods. We apply these schemes to the Uniaxial $\mathbf{Q}$-model in section 2.3.. Our numerical experiments in chapter 3. will show that the heavy-ball method gives a superior rate of convergence to a minimizer than the other schemes.

2.2.1. Classical Gradient Descent

Let X be a Banach space and $f : \mathrm{X} \to \mathbb{R}$ a differentiable function that is bounded below, so has a minimizer. Given the current guess x_k, the simplest form of *gradient descent* is to first compute a descent direction p_k:

$$a(p_k, v) = -\delta f[x_k](v) \quad \forall v \in \mathrm{X} \tag{2.22.}$$

where $a(\cdot,\cdot) : \mathrm{X} \times \mathrm{X} \to \mathbb{R}$ is some appropriate, coercive bilinear form that is an inner product on X. Then, update the guess:

$$x_{k+1} := x_k + \alpha p_k \tag{2.23.}$$

for some step size $\alpha > 0$. This procedure is iterated until some convergence criteria is achieved, such as $\|\delta f[x_k]\|_{\mathrm{X}^*} < \varepsilon_{\mathrm{tol}}$, for some tolerance $\varepsilon_{\mathrm{tol}} > 0$.

Choosing α appropriately, or using a line-search [54], yields a robust method but is usually quite slow to converge. The form of f can force the step size to be very small in order to ensure decrease of f, which is the case for the energy functional in (2.21.).

The standard approach can be improved by choosing $a(\cdot,\cdot)$ so that it is "matched" to δf, or by making the descent solve "more implicit." The later approach is motivated by *minimizing*

movements [55], and is described more in the next section.

2.2.2. Accelerated Gradient Descent

Algorithm 1 describes the minimizing movements strategy for gradient descent. It also includes a "momentum" term, known as the "heavy-ball" method (see [56] for the original method).

Algorithm 1 Minimizing movement gradient descent with momentum term.

Set a tolerance $\varepsilon_{\text{tol}} > 0$, initial guess $x_0 \in \mathrm{X}$, and set $k := 0$; choose $\gamma > 0$ and $\beta \geq 0$.
For $k \geq 0$, do the following.

1. Define the auxiliary function $\mathrm{G}_k[p] := (1/2)\,\|p\|_a^2 + \gamma f[x_k + p] - \beta a(p_{k-1}, p)$.
2. Let $p_k \in \mathrm{X}$ be the minimizer of $\mathrm{G}_k[\cdot]$, i.e. p_k solves

$$a(p_k, v) = -\gamma\, \delta f[x_k + p_k](v) + \beta a(p_{k-1}, v), \text{ for all } v \in \mathrm{X}, \tag{2.24.}$$

   i.e. p_k is a descent direction.
3. Update: $x_{k+1} := x_k + \alpha p_k$, for some step size $\alpha > 0$. Replace $k \leftarrow k + 1$.
4. If $\|\delta f[x_k]\|_{\mathrm{X}^*} < \varepsilon_{\text{tol}}$, then stop; else, return to Step 1.

Setting $\beta = 0$, since p_k minimizes $\mathrm{G}_k[\cdot]$, choosing $\alpha = 1$, we see that $f[x_{k+1}] = f[x_k + p_k] < (1/2)\,\|p_k\|_a^2 + f[x_k + p_k] = \mathrm{G}_k[p_k] \leq \mathrm{G}_k[0] = f[x_k]$, i.e. each step is guaranteed to decrease the functional. Choosing $\gamma > 0$ sufficiently small ensures that $\mathrm{G}_k[\cdot]$ is convex.

If $\beta > 0$, then this adds a bias term that influences the current search direction to follow the old search direction (i.e. an inertial term). It has been demonstrated, both theoretically and in practice, that the heavy-ball method can alleviate the "zig-zagging" behavior of classical gradient descent [56]. Of course, if $\beta > 0$, then strict decrease of the function is not guaranteed, unless a line-search is used.

Another accelerated gradient descent method is the well-known Nesterov method [57], which is described in Algorithm 2.

2.3. Accelerated Descent Schemes for the Uniaxial Q-model

The energy functional $\mathrm{E}^h_{\text{uni}}[s_h, \boldsymbol{\Theta}_h]$ in (2.21.) is non-convex. However, fixing either of the variables, and linearizing with respect to the other variable, yields a simple quadratic mini-

Algorithm 2 Nesterov's gradient descent.

Set a tolerance $\varepsilon_{\text{tol}} > 0$, initial guess $x_0 \in \mathrm{X}$, $x_{-1} := x_0$, $a_{-1} := 1$, and set $k := 0$; choose $\gamma > 0$. For $k \geq 0$, do the following.

1. Compute auxiliary point. Let $a_k = (1 + \sqrt{4a_{k-1}^2 + 1})/2$, and set $\beta_k = (a_{k-1} - 1)/a_k$. Then, compute $y_k = x_k + \beta_k(x_k - x_{k-1})$.
2. Compute search direction. Let $p_k \in \mathrm{X}$ solve
$$a(p_k, v) = -\gamma \delta f[y_k + p_k](v), \text{ for all } v \in \mathrm{X}. \tag{2.25.}$$
3. Update: $x_{k+1} := y_k + \alpha p_k$, for some step size $\alpha > 0$. Replace $k \leftarrow k + 1$.
4. If $\|\delta f[x_k]\|_{\mathrm{X}^*} < \varepsilon_{\text{tol}}$, then stop; else, return to Step 1.

mization to solve. Therefore, we use an alternating direction method to find minimizers of $\mathrm{E}^h_{\text{uni}}[s_h, \boldsymbol{\Theta}_h]$.

2.3.1. Tangential Variations

Any minimization strategy must account for the constraint $\boldsymbol{\Theta}_h(x_i) \in \mathrm{L}^{d-1}$, for all $x_i \in \mathcal{N}_h$, in (2.17.). We do this by computing variational derivatives that preserve the constraint to first order, i.e. we take variations tangential to the constraint manifold. Since $\boldsymbol{\Theta} \in \mathrm{L}^{d-1}$ is characterized by $\boldsymbol{\Theta} = \mathbf{n} \otimes \mathbf{n}$, we first do a Taylor expansion of $\mathbf{n}/|\mathbf{n}|$ in the direction of $\mathbf{v}$, where $\mathbf{v} \cdot \mathbf{n} = 0$ [1], i.e.

$$\mathbf{f}(\mathbf{v}) := \frac{\mathbf{n} + \mathbf{v}}{|\mathbf{n} + \mathbf{v}|} \quad \Rightarrow \quad \mathbf{f}(\mathbf{v}) = \mathbf{n} + \mathbf{v} - \frac{1}{2}|\mathbf{v}|^2\mathbf{n} + o(|\mathbf{v}|^2). \tag{2.26.}$$

The first variation of $\mathbf{n} \in \mathbb{S}^{d-1}$, in the direction $\mathbf{v}$, is then $\delta\mathbf{n}(\mathbf{v}) := \frac{d}{d\epsilon}\mathbf{f}(\epsilon\mathbf{v})\Big|_{\epsilon=0} = \mathbf{v} \in \mathrm{T}_{\mathbf{n}}\mathbb{S}^{d-1}$ (the tangent space of $\mathbb{S}^{d-1}$ at $\mathbf{n}$). Expanding $(\mathbf{n}/|\mathbf{n}|) \otimes (\mathbf{n}/|\mathbf{n}|)$ we get

$$\frac{\mathbf{n} + \mathbf{v}}{|\mathbf{n} + \mathbf{v}|} \otimes \frac{\mathbf{n} + \mathbf{v}}{|\mathbf{n} + \mathbf{v}|} = \left(1 - \frac{1}{2}|\mathbf{v}|^2\right)^2 \mathbf{n} \otimes \mathbf{n} + \mathbf{n} \otimes \mathbf{v} + \mathbf{v} \otimes \mathbf{n} + \mathbf{v} \otimes \mathbf{v} + o(|\mathbf{v}|^2), \tag{2.27.}$$

and the first variation of $\boldsymbol{\Theta} \in \mathrm{L}^{d-1}$, in the direction $\mathbf{v}$, is $\delta\boldsymbol{\Theta}(\mathbf{v}) = \mathbf{n} \otimes \mathbf{v} + \mathbf{v} \otimes \mathbf{n} \in \mathrm{T}_{\boldsymbol{\Theta}}\mathrm{L}^{d-1}$ (the tangent space of L^{d-1} at $\boldsymbol{\Theta}$). Thus, at $\boldsymbol{\Theta} = \mathbf{n} \otimes \mathbf{n}$, there is a bijection between $\mathrm{T}_{\boldsymbol{\Theta}}\mathrm{L}^{d-1}$ and $\mathrm{T}_{\mathbf{n}}\mathbb{S}^{d-1}$ [34].

Therefore, let us introduce the space of continuous, piecewise linear, vector-valued functions

$\mathbb{V}_h = \{\mathbf{v}_h \in [\mathrm{H}^1(\Omega)]^d : \mathbf{v}_h|_{\mathrm{T}} \in \mathcal{P}_1(\mathrm{T}), \forall \mathrm{T} \in \mathcal{T}_h\}$, and define the space of (discrete) tangential variations of $\boldsymbol{\Theta}_h = \mathbf{n}_h \otimes \mathbf{n}_h$ by

$$\begin{aligned}
&\mathbb{W}_h^{\perp}(\mathbf{n}_h) = \{\mathbf{v}_h \in \mathbb{V}_h : \mathbf{v}_h(x_i) \cdot \mathbf{n}_h(x_i) = 0, \text{ for all } x_i \in \mathcal{N}_h\},\\
&\mathbb{W}_h^{\perp}(\boldsymbol{\Theta}_h) = \{\mathbf{W}_h \in \overline{\mathbb{U}}_h : \mathbf{W}_h(x_i) = \mathbf{n}_h(x_i) \otimes \mathbf{v}_h(x_i) + \mathbf{v}_h(x_i) \otimes \mathbf{n}_h(x_i), \text{ where } \mathbf{v}_h \in \mathbb{W}_h^{\perp}(\mathbf{n}_h)\}.
\end{aligned} \tag{2.28.}$$

2.3.2. Discrete Variational Derivatives

Given $k \geq 0$, let $(s_h^k, \boldsymbol{\Theta}_h^k) \in \mathcal{A}_{\mathrm{uni}}^h(g_h, \mathbf{M}_h)$ and we write

$$s_i^k := s_h^k(x_i), \quad \boldsymbol{\Theta}_i^k := \boldsymbol{\Theta}_h^k(x_i), \quad \mathbf{n}_i^k := \mathbf{n}_h^k(x_i), \quad z_i := z_h(x_i), \quad \mathbf{v}_i := \mathbf{v}_h(x_i).$$

The discrete variational derivatives of the energy are given by

$$\begin{aligned}
\delta_{\boldsymbol{\Theta}} \mathrm{E}_{\mathrm{uni}}^h[s_h^k, \boldsymbol{\Theta}_h^k](\mathbf{W}_h) &= \frac{1}{2} \delta_{\boldsymbol{\Theta}} \mathring{\mathrm{E}}_{\mathrm{uni}}^h[s_h^k, \boldsymbol{\Theta}_h^k](\mathbf{W}_h),\\
\delta_{\boldsymbol{\Theta}} \mathring{\mathrm{E}}_{\mathrm{uni}}^h[s_h^k, \boldsymbol{\Theta}_h^k](\mathbf{W}_h) &= \sum_{i,j=1}^{\mathrm{N}} k_{ij} \left(\frac{(s_i^k)^2 + (s_j^k)^2}{2} \right) (\delta_{ij} \boldsymbol{\Theta}_h^k) : (\delta_{ij} \mathbf{W}_h),
\end{aligned} \tag{2.29.}$$

for all $\mathbf{W}_h \in \mathbb{W}_h^{\perp}(\boldsymbol{\Theta}_h)$, and

$$\begin{aligned}
\delta_s \mathrm{E}_{\mathrm{uni}}^h[s_h^k, \boldsymbol{\Theta}_h^k](z_h) &= \frac{d-1}{d} (\nabla s_h^k, \nabla z_h) + \frac{1}{2} \delta_s \mathring{\mathrm{E}}_{\mathrm{uni}}^h[s_h^k, \boldsymbol{\Theta}_h^k](z_h) + \frac{1}{\epsilon_{\mathrm{dw}}^2} (\psi'_{\mathrm{LdG}}(s_h^k), z_h),\\
\delta_s \mathring{\mathrm{E}}_{\mathrm{uni}}^h[s_h^k, \boldsymbol{\Theta}_h^k](z_h) &= \sum_{i,j=1}^{\mathrm{N}} k_{ij} |\delta_{ij} \boldsymbol{\Theta}_h^k|^2 \left(\frac{s_i^k z_i + s_j^k z_j}{2} \right).
\end{aligned} \tag{2.30.}$$

for all $z_h \in \mathbb{S}_h$. Note that $\delta_{\boldsymbol{\Theta}} \mathring{\mathrm{E}}_{\mathrm{uni}}^h[s_h^k, \boldsymbol{\Theta}_h^k](\mathbf{W}_h)$ is linear with respect to $\boldsymbol{\Theta}_h^k$ and $\mathbf{W}_h$ (separately), and $\delta_s \mathring{\mathrm{E}}_{\mathrm{uni}}^h[s_h^k, \boldsymbol{\Theta}_h^k](z_h)$ is linear with respect to s_h^k and z_h (separately). As will become clear in the next section, alternating the update of s_h and $\boldsymbol{\Theta}_h$ yields a convex problem to solve at each step, combined with a simple projection.

2.3.3. Minimization Algorithms

The minimization schemes consist of an outer loop within which three stages are performed. The first stage updates $\mathbf{\Theta}_h$ using one (accelerated) gradient descent step. The second stage projects $\mathbf{\Theta}_h$ onto the admissible set $\mathcal{A}^h_{\text{uni}}(g_h, \mathbf{M}_h)$ to enforce the constraint $\mathbf{\Theta}_h(x_i) = \mathbf{n}_h(x_i) \otimes \mathbf{n}_h(x_i)$ at the nodes of the mesh. The third stage updates s_h using one (accelerated) gradient descent step.

The inner products we use for computing descent directions are as follows. Given a function $\omega \in \mathrm{L}^\infty(\Omega)$ with $\omega \geq 0$, define the weighted space $\mathrm{H}^1_\omega(\Omega)$ through the norm

$$\|\mathbf{v}\|_{\mathrm{H}^1_\omega(\Omega)} := \left(\int_\Omega |\mathbf{v}(x)|^2 \, dx + \int_\Omega |\nabla \mathbf{v}(x)|^2 \, \omega(x) \, dx \right)^{1/2},$$

and write $(\cdot,\cdot)_{\mathrm{H}^1_\omega(\Omega)}$ as its inner product. When updating $\mathbf{n}_h$ (equivalently, $\mathbf{\Theta}_h$), we define $a^k_{\mathbf{n}}(\mathbf{t},\mathbf{v}) = (\mathbf{t},\mathbf{v})_{\mathrm{H}^1_{\omega^k}(\Omega)}$, with weight $\omega^k = (s^k_h)^2$. For updating s_h, we choose $a_s(\cdot,\cdot) = (\cdot,\cdot)$, the $\mathrm{L}^2(\Omega)$ inner product.

In order to obtain a linear system when updating s_h, we use the following convex splitting technique for ψ_{LdG} [58–60]. From (2.3.) and (2.9.), ψ_{LdG} has the form $\psi_{\mathrm{LdG}}(s) = \mathrm{K} + b_2 s^2 - b_3 s^3 + b_4 s^4$, where $b_2 \leq 0$, and $b_3, b_4 > 0$. Thus, writing $\psi_{\mathrm{LdG}}(s) = \left[\mathrm{K} + \mathrm{D}s^2\right] - \left[(\mathrm{D} - b_2)s^2 + b_3 s^3 - b_4 s^4\right] =: \psi_c(s) - \psi_e(s)$, we have that ψ_c, ψ_e are convex for all $s \in [-\frac{1}{d-1}, 1]$ provided $\mathrm{D} > 0$ is large enough. We then use the following approximation when computing a descent direction:

$$\left(\psi'_{\mathrm{LdG}}(s^k_h + r^k_h), z_h\right) := \left(\psi'_c(r^k_h), z_h\right) + \left(\psi'_c(s^k_h) - \psi'_e(s^k_h), z_h\right), \tag{2.31.}$$

where the first term on the right is linear in r^k_h. The first scheme we consider is given in Algorithm 3.

Algorithm 3 Descent scheme for $\mathrm{E}^h_{\mathrm{uni}}[s_h, \boldsymbol{\Theta}_h]$ with momentum term.

Set a tolerance $\varepsilon_{\mathrm{tol}} > 0$, initial guess $(s_h^0, \boldsymbol{\Theta}_h^0) \in \mathcal{A}^h_{\mathrm{uni}}(g_h, \mathbf{M}_h)$, with $\boldsymbol{\Theta}_h^0 = \mathrm{I}_h\left\{\mathbf{n}_h^0 \otimes \mathbf{n}_h^0\right\}$.

Set $\mathbf{t}_h^{-1} = \mathbf{0}$, $r_h^{-1} = 0$, and set $k := 0$; choose $\gamma_{\mathbf{n}}, \gamma_s > 0$ and $\beta_{\mathbf{n}}, \beta_s \geq 0$.

For $k \geq 0$, do the following.

1. Tangential search direction for $\mathbf{n}_h^k$. Find $\mathbf{t}_h^k \in \mathbb{W}_h^{\perp}(\mathbf{n}_h^k) \cap \mathrm{H}^1_{\Gamma_{\boldsymbol{\Theta}}}(\Omega)$ and $\mathbf{T}_h^k = \mathbf{n}_h^k \otimes \mathbf{t}_h^k + \mathbf{t}_h^k \otimes \mathbf{n}_h^k \in \mathbb{W}_h^{\perp}(\boldsymbol{\Theta}_h^k)$, such that

$$\begin{aligned} a_{\mathbf{n}}^k\left(\mathbf{t}_h^k, \mathbf{v}_h\right) = -\gamma_{\mathbf{n}}\delta_{\boldsymbol{\Theta}}\mathring{\mathrm{E}}^h_{\mathrm{uni}}[s_h^k, \boldsymbol{\Theta}_h^k + \mathbf{T}_h^k](\mathbf{V}_h) + \beta_{\mathbf{n}} a_{\mathbf{n}}^k\left(\mathbf{t}_h^{k-1}, \mathbf{v}_h\right), \\ \forall \mathbf{V}_h = \mathbf{n}_h^k \otimes \mathbf{v}_h + \mathbf{v}_h \otimes \mathbf{n}_h^k,\ \mathbf{v}_h \in \mathbb{W}_h^{\perp}(\mathbf{n}_h^k) \cap \mathrm{H}^1_{\Gamma_{\boldsymbol{\Theta}}}(\Omega). \end{aligned} \tag{2.32.}$$

2. Update $\mathbf{n}_h^k$. Let $\tilde{\mathbf{n}}_h^{k+1} \in \mathbb{V}_h$ with $\tilde{\mathbf{n}}_h^{k+1} := \mathbf{n}_h^k + \alpha_{\mathbf{n}}\mathbf{t}_h^k$, where $\alpha_{\mathbf{n}} > 0$ is the step size (either chosen arbitrarily or found by an exact line-search).

3. Update $\boldsymbol{\Theta}_h^k$ by *projection*. Compute $\boldsymbol{\Theta}_h^{k+1} \in \mathbb{T}_h(\Gamma_{\boldsymbol{\Theta}}, \mathbf{M}_h)$ with

$$\boldsymbol{\Theta}_h^{k+1}(x_i) := \frac{\tilde{\mathbf{n}}_h^{k+1}(x_i)}{|\tilde{\mathbf{n}}_h^{k+1}(x_i)|} \otimes \frac{\tilde{\mathbf{n}}_h^{k+1}(x_i)}{|\tilde{\mathbf{n}}_h^{k+1}(x_i)|}, \quad \forall x_i \in \mathcal{N}_h. \tag{2.33.}$$

4. Search direction for s_h^k. Find $r_h^k \in \mathbb{S}_h(\Gamma_s, 0)$ such that, for all $z_h \in \mathbb{S}_h(\Gamma_s, 0)$,

$$\begin{aligned} a_s\left(r_h^k, z_h\right) &= -\gamma_s\delta_s \mathrm{E}^h_{\mathrm{uni}}[s_h^k + r_h^k, \boldsymbol{\Theta}_h^{k+1}](z_h) + \beta_s a_s\left(r_h^{k-1}, z_h\right), \\ &\text{or} \\ a_s\left(r_h^k, z_h\right) + \gamma_s\delta_s \mathrm{E}^h_{\mathrm{uni-m}}[r_h^k, \boldsymbol{\Theta}_h^{k+1}](z_h) + \frac{\gamma_s}{\epsilon_{\mathrm{dw}}^2}\left(\psi_c'(r_h^k), z_h\right) \\ = -\gamma_s\delta_s \mathrm{E}^h_{\mathrm{uni-m}}[s_h^k, \boldsymbol{\Theta}_h^{k+1}](z_h) - \frac{\gamma_s}{\epsilon_{\mathrm{dw}}^2}\left(\psi'_{\mathrm{LdG}}(s_h^k), z_h\right) + \beta_s a_s\left(r_h^{k-1}, z_h\right). \end{aligned} \tag{2.34.}$$

5. Update s_h^k. Let $s_h^{k+1} \in \mathbb{S}_h(\Gamma_s, g_h)$ with $s_h^{k+1} := s_h^k + \alpha_s r_h^k$, where $\alpha_s > 0$ is the step size (either chosen arbitrarily or found by an exact line-search).

6. If $\max\left(\|\mathbf{t}_h^k\|_{\mathrm{L}^\infty(\Omega)}, \|r_h^k\|_{\mathrm{L}^\infty(\Omega)}\right) < \varepsilon_{\mathrm{tol}}$, then stop; else, replace $k \leftarrow k+1$ and return to Step 1.

The following special case of Algorithm 3 is equivalent to the method in [34]: set $\gamma = \delta t$ (time-step), $\beta = 0$ and $\alpha = 1$ (in both updates). The resulting algorithm is monotonically energy decreasing [34, Thm. 2], if $\delta t < \mathrm{C}h^{d/2}$ for some constant $\mathrm{C} > 0$, i.e.

$$\mathrm{E}^h_{\mathrm{uni}}[s^{\mathrm{N}}_h, \boldsymbol{\Theta}^{\mathrm{N}}_h] + \frac{1}{\delta t}\left(\sum_{k=0}^{\mathrm{N}-1} \|\mathbf{t}^k_h\|^2_{\mathrm{H}^1_{(s^k_h)^2}(\Omega)} + \|r^k_h\|^2_{\mathrm{L}^2(\Omega)}\right) \leq \mathrm{E}^h_{\mathrm{uni}}[s^0_h, \boldsymbol{\Theta}^0_h] \quad \forall \mathrm{N} \geq 1.$$

The reason for the time step restriction is due to the "second order inconsistency" in updating $\boldsymbol{\Theta}^k_h$ in (2.32.). In other words, setting $\widetilde{\boldsymbol{\Theta}}^{k+1}_h := \boldsymbol{\Theta}^k_h + \mathbf{T}^k_h$, it is clear that $\widetilde{\boldsymbol{\Theta}}^{k+1}_h(x_i) \neq \mathbf{a} \otimes \mathbf{a} \in \mathrm{L}^{d-1}$, for *any* $\mathbf{a} \in \mathbb{S}^{d-1}$ and any node $x_i \in \mathcal{N}_h$. According to (2.27.), a better option would be to replace $\boldsymbol{\Theta}^k_h + \mathbf{T}^k_h$ with

$$\mathbf{n}^k_h \otimes \mathbf{n}^k_h + \mathbf{n}^k_h \otimes \mathbf{t}^k_h + \mathbf{t}^k_h \otimes \mathbf{n}^k_h + \mathbf{t}^k_h \otimes \mathbf{t}^k_h \equiv \left(\mathbf{n}^k_h + \mathbf{t}^k_h\right) \otimes \left(\mathbf{n}^k_h + \mathbf{t}^k_h\right), \tag{2.35.}$$

in (2.32.), but (2.35.) is nonlinear. In Section 2.3.4., we show that (2.35.) can be accounted for by an exact line search with negligible computational cost.

2.3.4. Energy Decrease and Exact Line Search

Setting a fixed step size for $\alpha_{\mathbf{n}}$ and/or α_s is simple, but does not guarantee decrease of the energy at each iteration. Hence, we propose an exact line search. Because of the simple form of $\mathring{\mathrm{E}}^h_{\mathrm{uni}}[s^k_h, \boldsymbol{\Theta}^k_h]$, we have that

$$\ell_{\mathbf{n}}(\xi) = \mathring{\mathrm{E}}^h_{\mathrm{uni}}[s^k_h, \left(\mathbf{n}^k_h + \xi \mathbf{t}^k_h\right) \otimes \left(\mathbf{n}^k_h + \xi \mathbf{t}^k_h\right)], \tag{2.36.}$$

is a quartic polynomial in ξ. So given $s^k_h, \mathbf{n}^k_h, \mathbf{t}^k_h$, we can recover $\ell_{\mathbf{n}}(\xi)$ by sampling at five points. It is then a trivial computation to find the value of ξ that minimizes $\ell_{\mathbf{n}}(\xi)$. Since $\mathring{\mathrm{E}}^h_{\mathrm{uni}}[s^k_h, \boldsymbol{\Theta}^k_h]$ is convex in $\boldsymbol{\Theta}^k_h$ (for fixed s^k_h), we are guaranteed to find a positive ξ value that minimizes $\ell_{\mathbf{n}}$, unless $\mathring{\mathrm{E}}^h_{\mathrm{uni}}[s^k_h, \mathbf{n}^k_h \otimes \mathbf{n}^k_h]$ is already a minimum; note that

$$\left(\mathbf{n}^k_h + \mathbf{t}^k_h\right) \otimes \left(\mathbf{n}^k_h + \mathbf{t}^k_h\right) \approx \boldsymbol{\Theta}^k_h + \mathbf{T}^k_h,$$

for $|\mathbf{t}_h^k|$ sufficiently small and $\boldsymbol{\Theta}_h^k + \mathbf{T}_h^k$ is *linear* in $\mathbf{t}_h^k$.

Moreover, $\mathrm{E}_{\mathrm{uni}}^h[s_h^{k+1}, \boldsymbol{\Theta}_h^{k+1}]$, also has a simple form, i.e. fixing $\boldsymbol{\Theta}_h^{k+1}$,

$$\ell_s(\xi) = \mathrm{E}_{\mathrm{uni}}^h[s_h^k + \xi r_h^k, \boldsymbol{\Theta}_h^{k+1}] \tag{2.37.}$$

is a quartic polynomial in ξ because of ψ_{LdG}. Hence, we can easily do an exact line search when updating s_h^k as above. In the next section, we show the efficacy of this approach.

Chapter 3.
Numerical Experiments

In this chapter, the minimization algorithms described in chapter 2. were used to compute the minimizers of the one-constant Landau-de Gennes energy functional given in Equation 2.2. with the uniaxial constraints enforced. The minimizers were computed with and without the line search method. The rate of convergence of the accelerated gradient descent algorithms were compared to the classical gradient descent algorithm.

The minimization methods were implemented using the MATLAB/C++ finite element toolbox FELICITY [61] to minimized the energy functional in the 2-D and 3-D simulations. In the numerical computations, the linear system was solved using the algebraic multi-grid solver - AGMG [62, 63] for the 3-D simulations, but the 2-D simulations used the MATLAB backslash command to solve the linear systems.

3.1. Experiment 1: Simulation of uniaxial constrained nematic liquid crystal in 2D

Considering the one-constant energy of a uniaxially constrained liquid crystal described in section 2.1., and a double well potential $\psi_{\mathrm{LdG}}(s)$ given as

$$\psi_{\mathrm{LdG}}(s) = \psi_c(s) - \psi_e(s) = 1 - 8.16325s^2 + 33.31945s^4 \tag{3.1.}$$

such that $\psi_c(s) = \mathrm{K} + \frac{(\mathrm{A}+\mathrm{D})}{2}s^2 + \frac{\mathrm{C}}{4}s^4$ and $\psi_e(s) = \frac{\mathrm{D}}{2}s^2 - \frac{\mathrm{C}}{4}s^4$ with $\mathrm{A} = -16.3265, \mathrm{C} = 66.6389, \mathrm{D} = 144.040024,$ and $\mathrm{K} = 1.0$.

The Dirichlet boundary conditions imposed on the liquid crystal domain is

$$\begin{aligned} s &= s^* = 0.7, \text{ on} \quad \Gamma_s \\ \mathbf{n}(x,y) &= [\cos(\theta), \sin(\theta)]^{\mathrm{T}}, \theta = \operatorname{atan2}\left(\frac{y-y_0}{x-x_0}\right) \text{ on } \Gamma_{\boldsymbol{\Theta}} \end{aligned} \tag{3.2.}$$

where $\boldsymbol{\Theta} = \mathbf{n} \otimes \mathbf{n}$ is defined on $\Gamma_s, \Gamma_{\boldsymbol{\Theta}} = \partial\Omega$ and $[x_0, y_0]^{\mathrm{T}} = [0.5, 0.5]^{\mathrm{T}}$

The solutions were initialized with $s_0 = s^* = 0.7$, $\mathbf{n}_0(x,y) = [\cos(\theta_0), \sin(\theta_0)]^{\mathrm{T}}, \theta_0 = \operatorname{atan2}\left(\frac{y-y_0}{x-x_0}\right)$, $[x_0, y_0]^{\mathrm{T}} = [0.182, 0.31]^{\mathrm{T}}, \boldsymbol{\Theta}_0 = \mathbf{n}_0 \otimes \mathbf{n}_0$ The boundary and initial conditions

imposed on the LC domain is shown in Figure 3.1..

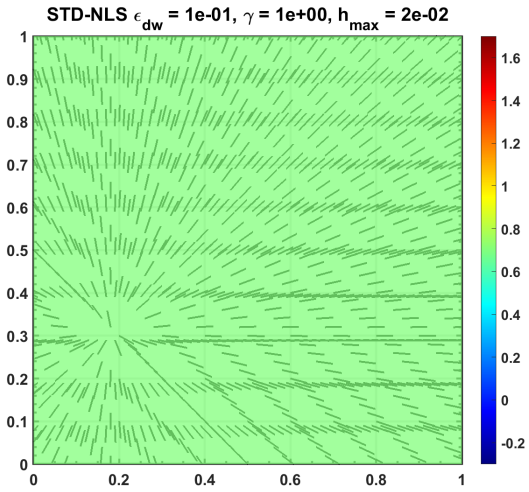

Figure 3.1. Initial state of the uniaxially constrained nematic LC - 2D.

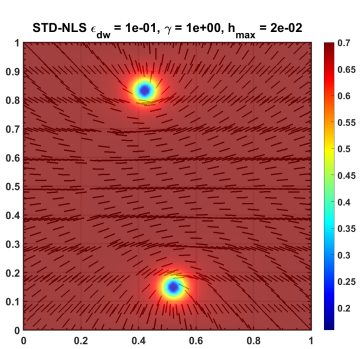

(a) Standard gradient descent algorithm

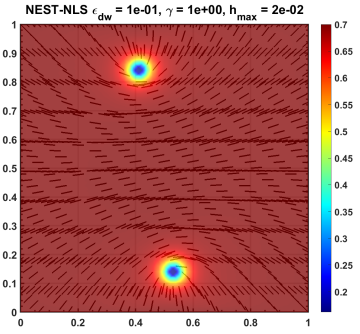

(b) Nesterov accelerated gradient descent algorithm

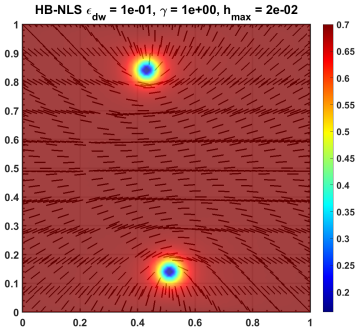

(c) Heavy-Ball accelerated gradient descent algorithm

Figure 3.2. Solution of each algorithm without using exact line search method for $\epsilon_{dw} = 1 \times 10^{-1}$, $\gamma = 1$, and $h_{\mathrm{D}} = 2 \times 10^{-2}$

Figure 3.2. and Figure 3.3. shows the minimizers of the uniaxially constrained liquid crystal

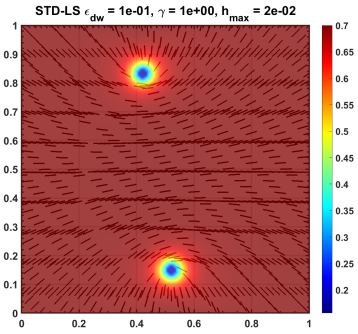

(a) Standard gradient descent algorithm

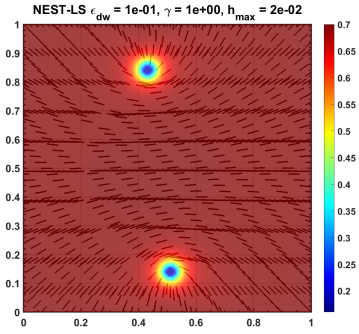

(b) Nesterov accelerated gradient descent algorithm

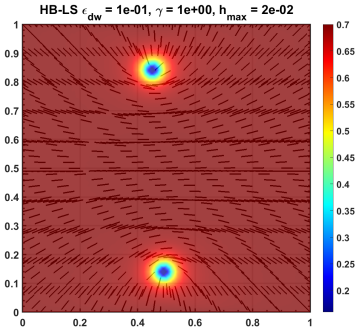

(c) Heavy-Ball accelerated gradient descent algorithm

Figure 3.3. Solution of each algorithm using exact line search method for $\epsilon_{dw} = 1 \times 10^{-1}$, $\gamma = 1$, and $h_{\mathrm{D}} = 2 \times 10^{-2}$

using the three gradient descent minimization schemes without and with exact line search method respectively as discussed in chapter 2.. Point defects observed in the liquid crystal domains were captured by the three schemes at locations that approximately agree among them.

Table 3.1. Minimized LDG Uniaxially Constrained LC Energy (Without Line Search) - $\gamma = 1, h_{\mathrm{D}} = 2 \times 10^{-2}, \alpha = 1$

ϵ_{dw}	STD	Heavy-Ball	Nesterov
1×10^{-1}	5.3184	5.3122	5.3133
2×10^{-1}	4.2571	4.2522	4.2571
4×10^{-1}	3.2300	3.2244	3.2281
5×10^{-1}	2.9241	2.9244	2.9255

The minimum energy of the liquid crystal computed using these algorithms as a function of the liquid crystal material properties ϵ_{dw} are tabulated in Table 3.1. and Table 3.2. for each minimization scheme without exact line search and with exact line search respectively. Figure 3.4. and

Table 3.2. Minimized LDG Uniaxially Constrained LC Energy (With Line Search) - $\gamma = 1, h_{\mathrm{D}} = 2\times10^{-2}$

ϵ_{dw}	STD	Heavy-Ball	Nesterov
1×10^{-1}	5.3184	5.3118	5.3122
2×10^{-1}	4.2571	4.2335	4.2571
4×10^{-1}	3.2281	3.2244	3.2243
5×10^{-1}	2.9236	2.9236	2.9252

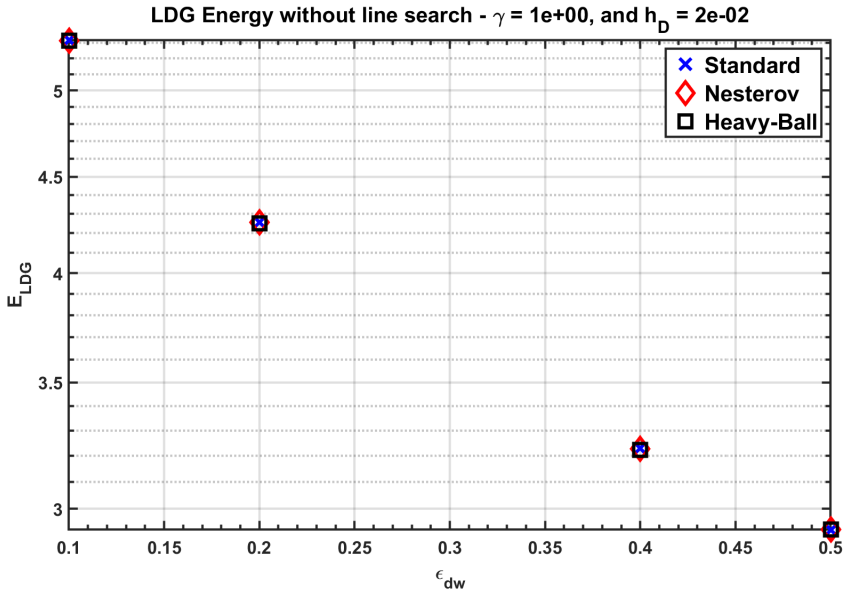

Figure 3.4. Minimized Landau-de Gennes energy of the constrained liquid crystal for each of the gradient descent algorithm - $\gamma = 1, h_{\mathrm{D}} = 2\times10^{-2}$.

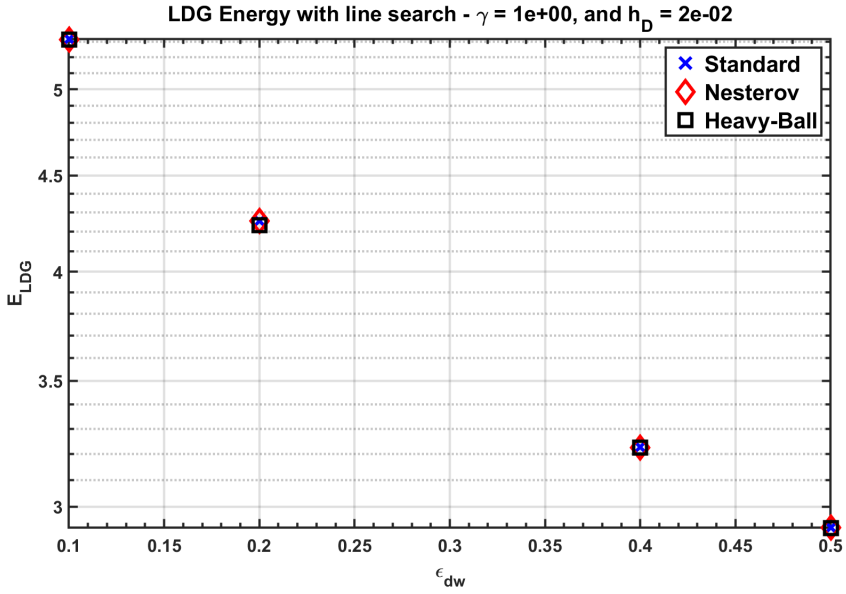

Figure 3.5. Minimized Landau-de Gennes energy of the constrained liquid crystal using the exact line search method with each of the gradient descent algorithm - $\gamma = 1, h_{\mathrm{D}} = 2\times10^{-2}$.

Figure 3.5. depicts the variation of the uniaxially constrained LC energy minimizers computed by each minimization scheme implemented without and with exact line search method respectively.

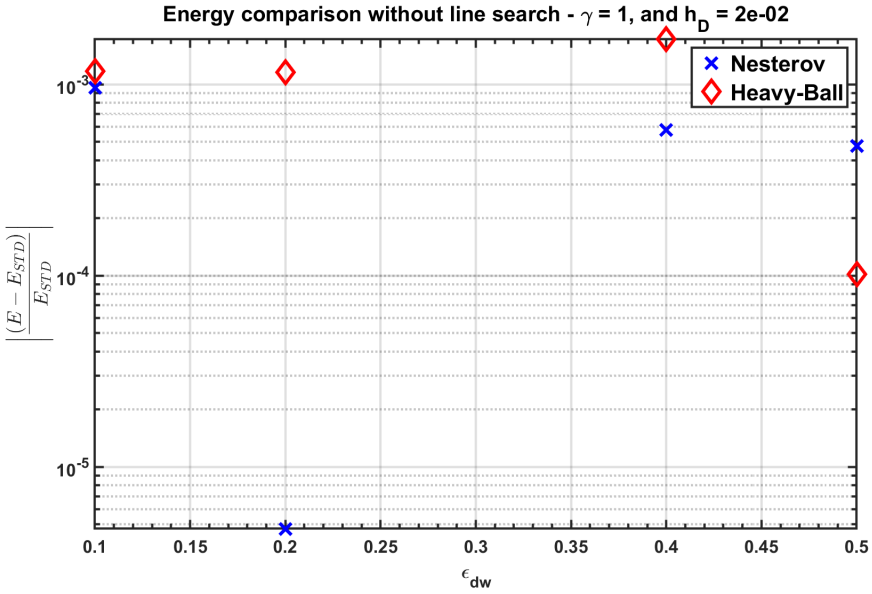

Figure 3.6. Comparison of the Minimized Landau-de Gennes energy of the constrained liquid crystal for each of the accelerated gradient descent algorithm wrt standard gradient descent without using the exact line search method - $\gamma = 1, h_{\mathrm{D}} = 2 \times 10^{-2}$.

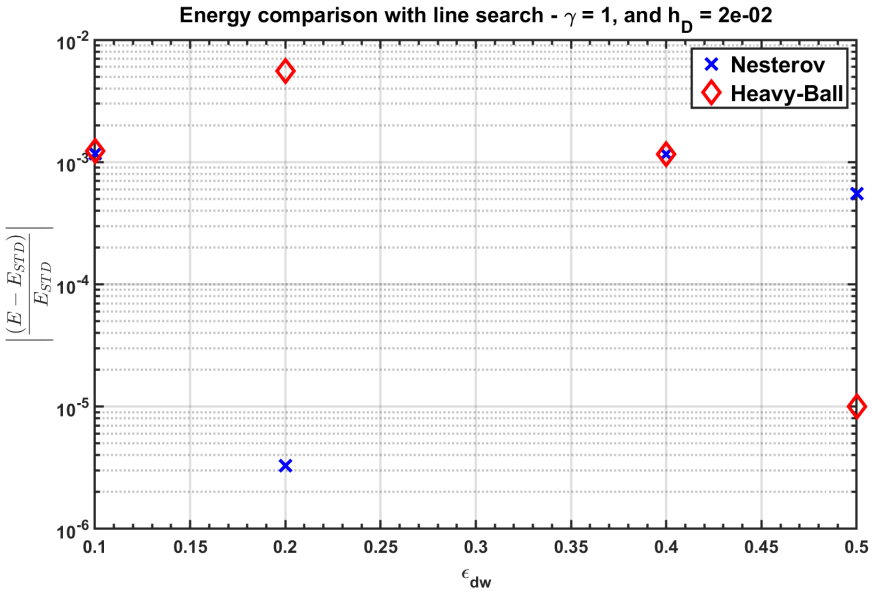

Figure 3.7. Comparison of the Minimized Landau-de Gennes energy of the constrained liquid crystal for each of the accelerated gradient descent algorithm wrt standard gradient descent using the exact line search method- $\gamma = 1, h_{\mathrm{D}} = 2 \times 10^{-2}$.

The energy of the equilibrium state of nematic liquid crystal computed using the accelerated gradient descent algorithm was compared to the minimized energy computed using the standard

gradient descent is shown in Figure 3.6. and Figure 3.7. without and with using the exact line search method repsectively.

As shown in the Figure 3.4. - Figure 3.5., the minimized energy of the equilibrium state of the nematic LCs are approximately similar using these schemes. This indicates that the schemes captured the behavior of the LC in the 2D domain. Moreover, the performance of these algorithms are measured with respect to the duration of computation and the number of iteration required to compute the equilibrium state of the nematic LC.

The performance of the gradient descent schemes were compared such that the liquid crystal material parameter $\epsilon_{dw} = [0.1, 0.2, 0.4, 0.5]$, and the algorithm parameter $\gamma = 1$ with the mesh diameter $h_{\mathrm{D}} = 2 \times 10^{-2}$.

3.1.1. Performance of the Heavy-Ball and Nesterov accelerated gradient descent algorithm

This section presents the performance of the accelerated gradient descent schemes - heavy-ball(HB) and Nesterov (NEST) - used in the minimization of the Landau-de Gennes one constant energy model of a uniaxially constrained nematic LC. The performance of the schemes with and without the exact line search method is quantitatively measured in terms of the number of iteration and duration of the computation. The implementation of the line search is labeled with LS while without the line search is labeled with NLS.

In the results presented, $\eta_{\mathrm{B}} = \epsilon_{dw}^2, \epsilon_{dw} = [0.1, 0.2, 0.4, 0.5]$ and $\gamma = 1$

Figure 3.8. depict the number of iterations needed for the computation to attain equilibrium. As shown, the Nesterov's method required the least amount of iterations to attain equilibrium state in comparison to the other gradient descent method. In addition to the performance of the accelerated gradient descent method w.r.t the other methods, the coupling of line search algorithm improved the performance of all the gradient descent schemes. The accelerated gradient descent schemes performed better in reducing the number of iterations required for the computation.

In terms of the duration of computing the equilibrium state of the nematic LC using the accelerated gradient descents, the computational time reduced when the accelerated gradient de-

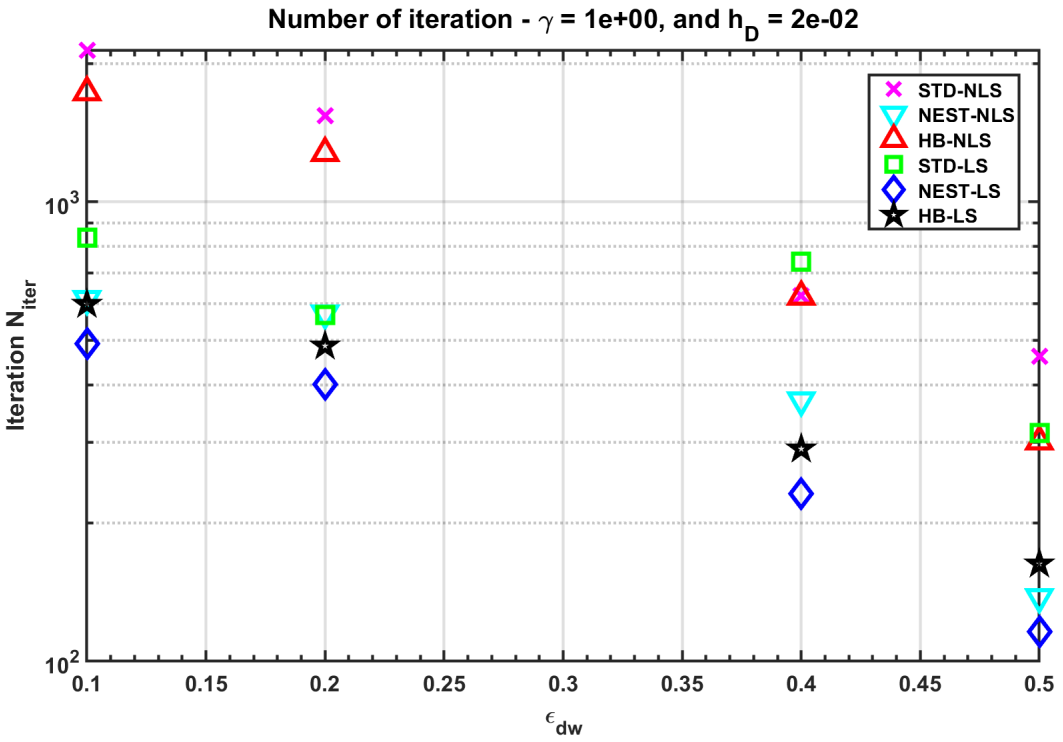

Figure 3.8. Comparison of the number of iterations required to attained the equilibrium state using the algorithms for the Computation such that $\gamma = 1$, and $h_{\mathrm{D}} = 2 \times 10^{-2}$

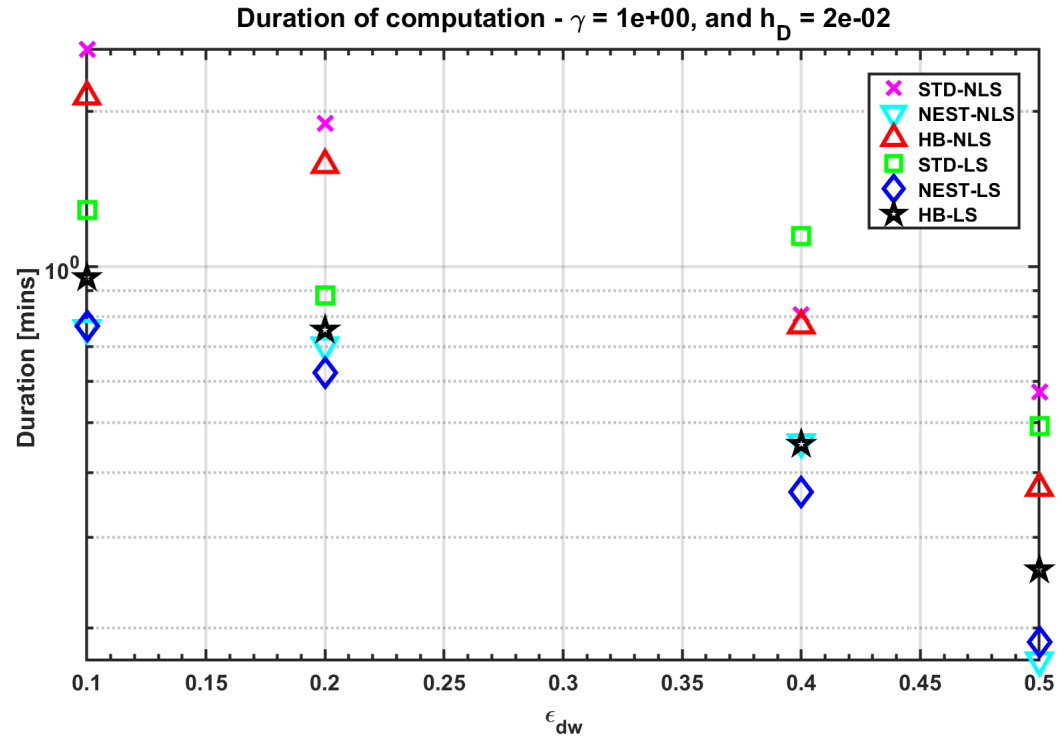

Figure 3.9. Comparison of the number of iterations required to attained the equilibrium state using the algorithms for the Computation such that $\gamma = 1$, and $h_{\mathrm{D}} = 2 \times 10^{-2}$

scent schemes are used for the computation. Figure 3.9. shows the duration of the computation using each algorithms for the computation. Similar to the number of iteration required for the computation, the duration of the computation decreased using the accelerated gradient descent in comparison to the classical gradient descent scheme. The Nesterov accelerated gradient descent scheme performed better than the Heavy-Ball gradient descent scheme.

3.2. Experiment 2: Simulation of uniaxial constrained nematic liquid crystal in 3D

Suppose the one-constant Landau-de Gennes energy of a uniaxially constrained liquid crystal described in section 2.1. is imposed on a domain $\Omega \in \mathbb{R}^3$, and a double well potential $\psi_{\mathrm{LdG}}(s)$ given as

$$\psi_{\mathrm{LdG}}(s) = \psi_c(s) - \psi_e(s) = 1 - 3.75104s^2 - 40.6504s^3 + 33.259425s^4 \tag{3.3.}$$

such that $\psi_c(s) = \mathrm{K} + \frac{(\mathrm{A}+\mathrm{D})}{2}s^2 - \frac{\mathrm{B}}{3}s^3 + \frac{\mathrm{C}}{4}s^4$ and $\psi_e(s) = \frac{\mathrm{D}}{2}s^2 + \frac{\mathrm{B}}{3}s^3 - \frac{\mathrm{C}}{4}s^4$ with $\mathrm{A} = -7.50208, \mathrm{B} = 60.9756, \mathrm{C} = 66.51885, \mathrm{D} = 552.22912,$ and $\mathrm{K} = 1.0$.

The domain Ω has a hole cut out such that its center is located at (x_c, y_c, z_c) and has a radius R. The Dirichlet boundary conditions imposed on the liquid crystal domain is

$$\begin{gathered} s = s^* = 0.7, \text{ on } \quad \Gamma_s = \partial\Omega \\ \mathbf{n}(x,y,z) = \begin{cases} \frac{\mathbf{n}_{bc}}{|\mathbf{n}_{bc}|} & \text{on } \Gamma_{\mathrm{H}ole} \\ [0,0,1]^{\mathrm{T}} & \text{on } \Gamma_{\boldsymbol{\Theta}} = \partial\Omega / \Gamma_{\mathrm{H}ole} \end{cases} \\ \boldsymbol{\Theta} = \mathbf{n} \otimes \mathbf{n} \text{ is defined on } \Gamma_s, \Gamma_{\boldsymbol{\Theta}} = \partial\Omega \end{gathered} \tag{3.4.}$$

where,$\mathbf{n}_{bc} = [x - x_c, y - y_c, z - z_c]^{\mathrm{T}}$, and $[x_c, y_c, z_c]^{\mathrm{T}} = [0.35355, 0.35355, 0]^{\mathrm{T}}, \mathrm{R}_{\mathrm{H}ole} = 0.20011$ The solutions were initialized with $s_0 = s^* = 0.7$,

$$\mathbf{n}_0(x,y) = \begin{cases} [0,0,1]^{\mathrm{T}} & \text{for } z \geq 0 \\ [0,0,-1]^{\mathrm{T}} & \text{for } z < 0 \end{cases}$$

$$\boldsymbol{\Theta}_0 = \mathbf{n}_0 \otimes \mathbf{n}_0 \quad \text{on } \Omega$$

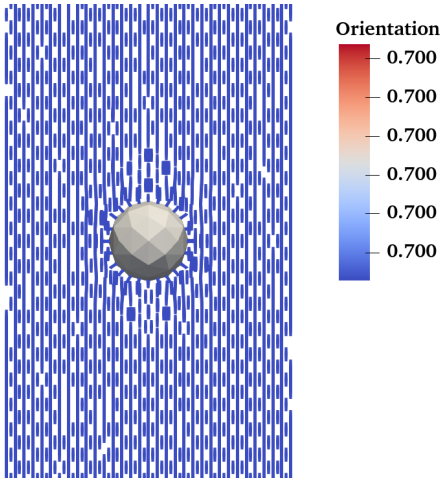

Figure 3.10. Initial state of the uniaxially constrained nematic LC - 3D.

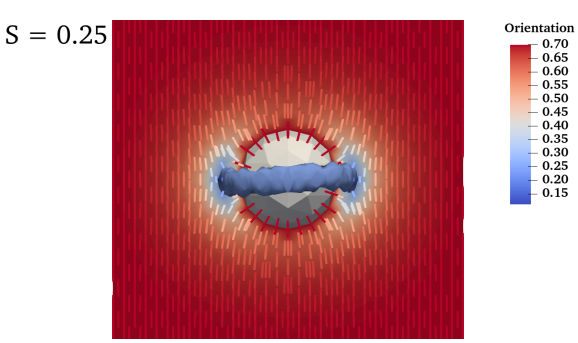

(a) Standard gradient descent algorithm

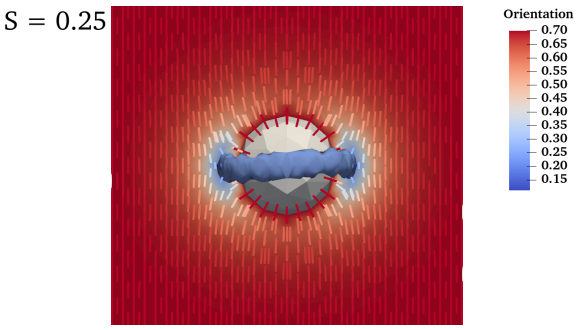

(b) Nesterov accelerated gradient descent algorithm

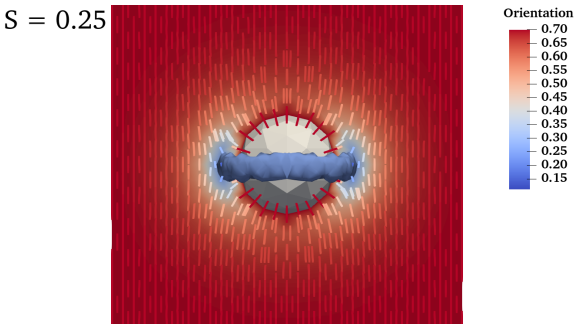

(c) Heavy-Ball accelerated gradient descent algorithm

Figure 3.11. Solution of each algorithm without using exact line search method for $\epsilon_{dw} = 1 \times 10^{-1}$, $\gamma = 1$

Figure 3.11. and Figure 3.12. shows the numerical results of the minimizer of the uniaxially constrained liquid crystal using the three gradient descent algorithms without and with exact line search method respectively in a 3-D domain.

The energy minimizers of the uniaxial constrained nematic LC using the gradient descent

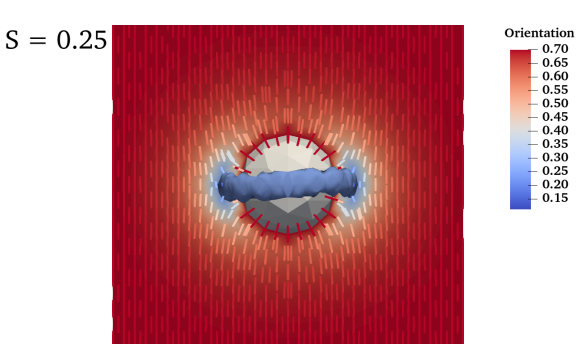

(a) Standard gradient descent algorithm

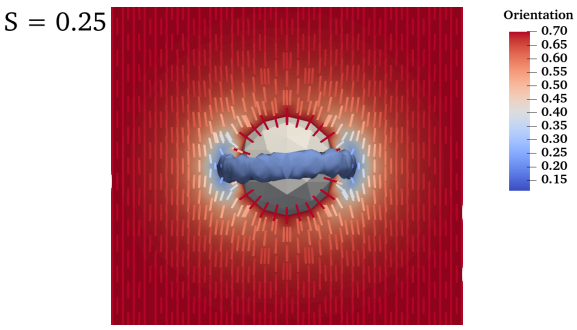

(b) Nesterov accelerated gradient descent algorithm

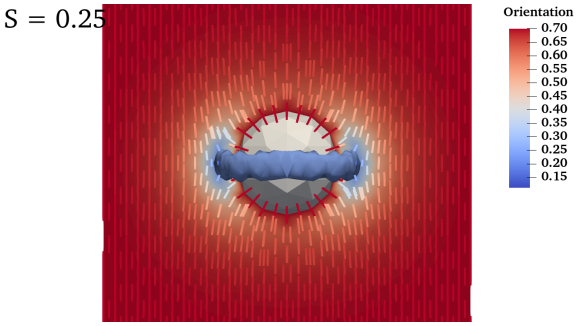

(c) Heavy-Ball accelerated gradient descent algorithm

Figure 3.12. Solution of each algorithm using exact line search method for $\epsilon_{dw} = 1 \times 10^{-1}$, $\gamma = 1$

Table 3.3. Minimized LDG Uniaxially Constrained LC Energy (Without Line Search 3D) - $\gamma = 1, h_{\mathrm{D}} = 6 \times 10^{-2}$, $\alpha = 1$

ϵ_{dw}	STD	Heavy-Ball	Nesterov
2×10^{-1}	2.9572	2.9572	2.9572
3×10^{-1}	2.7016	2.7016	2.7016
4×10^{-1}	2.5360	2.5360	2.5360
5×10^{-1}	2.4195	2.4193	2.4195

Table 3.4. Minimized LDG Uniaxially Constrained LC Energy (Without Line Search 3D) - $\gamma = 1, h_{\mathrm{D}} = 6 \times 10^{-2}$

ϵ_{dw}	STD	Heavy-Ball	Nesterov
2×10^{-1}	2.9572	2.9572	2.9572
3×10^{-1}	2.7016	2.7016	2.7016
4×10^{-1}	2.5360	2.5360	2.5360
5×10^{-1}	2.4195	2.4196	2.4195

schemes is tabulated in Table 3.3. and Table 3.4. without and with exact line search method implemented in the schemes respectively. The variation of the minimum energy of the uniaxially

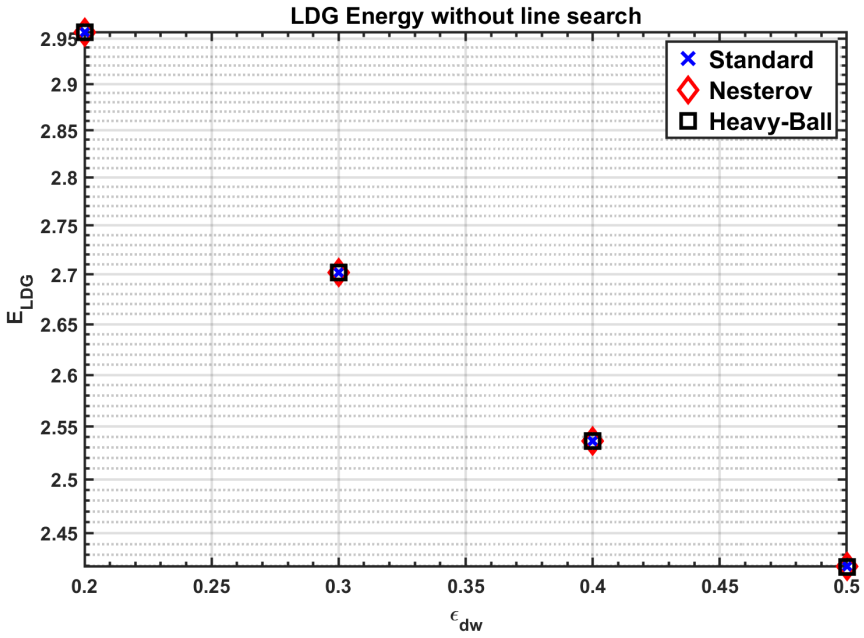

Figure 3.13. Minimized Landau-de Gennes energy of the constrained liquid crystal for each of the gradient descent algorithm - $\gamma = 1$.

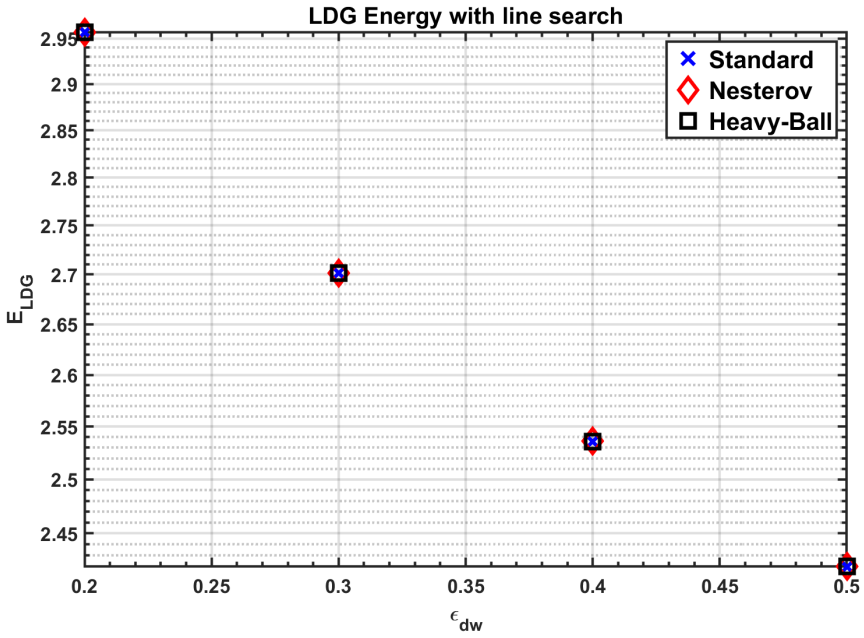

Figure 3.14. Minimized Landau-de Gennes energy of the constrained liquid crystal using the exact line search method with each of the gradient descent algorithm - $\gamma = 1$.

constrained neamtic LC computed using these schemes as a function of the liquid crystal material properties ϵ_{dw} are shown in Figure 3.13. and Figure 3.14. such that each schemes were implemented without and with exact line search method respectively. As depicted in the figures, the

energy minimizers of the nematic LC for these schemes are approximately the same.

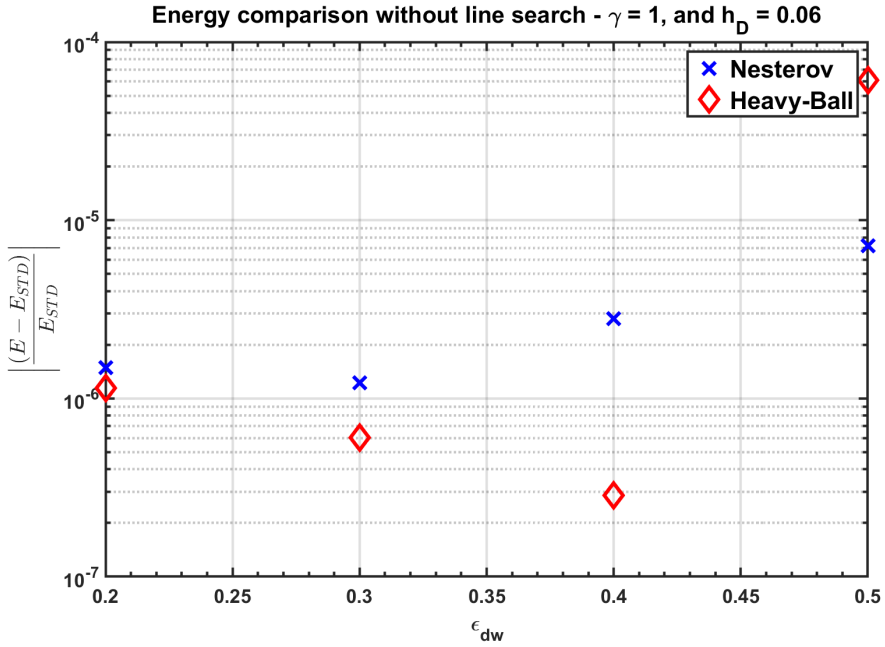

Figure 3.15. Comparison of the Minimized Landau-de Gennes energy of the constrained liquid crystal for each of the accelerated gradient descent algorithm wrt standard gradient descent without using the exact line search method - $\gamma = 1$.

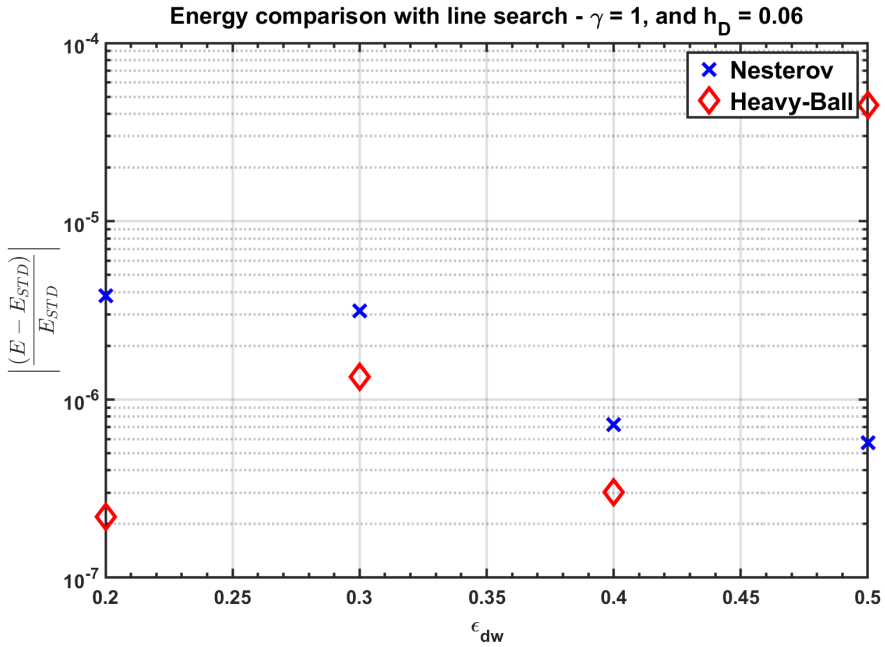

Figure 3.16. Comparison of the Minimized Landau-de Gennes energy of the constrained liquid crystal for each of the accelerated gradient descent algorithm wrt standard gradient descent using the exact line search method- $\gamma = 1$.

Figure 3.15. and Figure 3.16. compare the computed energy of the equilibrium state of ne-

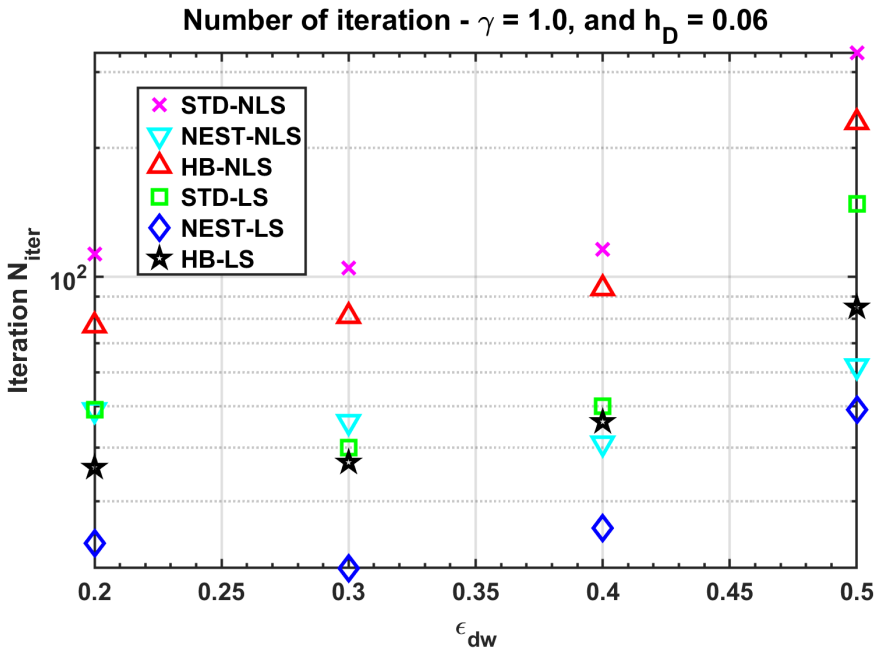

Figure 3.17. Number of iterations for computing the equilibrium state of the liquid crystal using the gradient descent schemes.

matic liquid crystal using the accelerated gradient descent algorithm to the minimized energy computed using the standard gradient descent without and with the use of exact line search method repsectively.

In Figure 3.13. - Figure 3.14., the minimized energy of the equilibrium state of nematic LCs computed using these algorithms approximately agree strictly to a high degree of accuracy. However, the energy of the equilibrium state computed using Heavy-ball accelerated gradient descent method is closer to the standard gradient descent scheme than the Nesterov gradient descent scheme.

3.2.1. Performance of the Accelerated Gradient Descent Schemes

In terms of the duration and number of iterations required to compute the equilibrium state of the uniaxially constrained nematic LC as shown in Figure 3.18. and Figure 3.17. respectively, the accelerated gradient descent schemes performed better than the classical gradient descent schemes. The computational time reduced when the accelerated gradient descent schemes are used for the computation. Similar to the duration of the computation, the number of iteration required for the computation decreased using the accelerated gradient descent in comparison

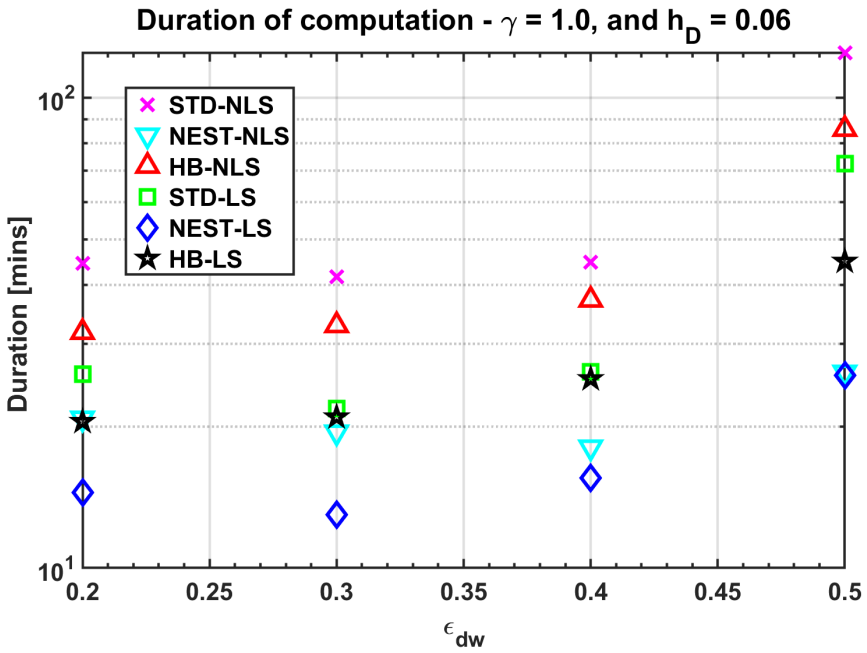

Figure 3.18. Duration of computing the equilibrium state of the liquid crystal using the gradient descent schemes.

to the classical gradient descent scheme. The Nesterov accelerated gradient descent scheme performed better than the Heavy-Ball gradient descent scheme.

Chapter 4.
Conclusion

Modeling of uniaxially constrained nematic liquid crystal has been studied using the Q-theory proposed by Landau-de Gennes. In this work, the one-constant unixaially constrained liquid crystal model was analyzed using three minimization schemes - standard gradient scheme, Heavy-ball accelerated gradient descent scheme and the Nesterov accelerated gradient descent schemes.

The energy minimizers computed by these minimization schemes are approximately similar. This indicates that these schemes computed almost the same energy state of the uniaxially constrained nematic LC.

The performance of the algorithms were measured based on the rate of convergence of the schemes and the duration required to ascertain the equilibrium state of a liquid crystal under certain conditions.

The minimization algorithms were implemented using a MATLAB/C++ toolbox FELICITY [61] and numerical experiments were conducted using the algorithms to compute the energy minimizer of nematic liquid crystal in 2D and 3D. Based on the numerical experiments, the accelerated algorithms - Nesterov and Heavy-ball - computed the energy minimizers with a higher convergence rate than the standard gradient descent method.

When the exact line search method was incorporated into these algorithms, the rate of convergence of the computation increased and the duration of the computation reduced for each algorithm.

References

[1] E. G. Virga. *Variational Theories for Liquid Crystals*, volume 8. Chapman and Hall, London, 1st edition, 1994.

[2] P. G. de Gennes and J. Prost. *The Physics of Liquid Crystals*, volume 83 of *International Series of Monographs on Physics*. Oxford Science Publication, Oxford, UK, 2nd edition, 1995.

[3] Jan P.F. Lagerwall and Giusy Scalia. A new era for liquid crystal research: Applications of liquid crystals in soft matter nano-, bio- and microtechnology. *Current Applied Physics*, 12(6):1387 – 1412, 2012. ISSN 1567-1739. doi: https://doi.org/10.1016/j.cap.2012.03.019. URL http://www.sciencedirect.com/science/article/pii/S1567173912001113.

[4] L.M. Blinov. *Electro-optical and magneto-optical properties of liquid crystals*. Wiley, 1983.

[5] J. W. Goodby. *Handbook of Visual Display Technology (Editors: Chen, Janglin, Cranton, Wayne, Fihn, Mark)*, chapter Introduction to Defect Textures in Liquid Crystals, pages 1290–1314. Springer, 2012.

[6] Jian Sun, Huihui Wang, Ling Wang, Hui Cao, Hui Xie, Xueyao Luo, Jiumei Xiao, Hangjun Ding, Zhou Yang, and Huai Yang. Preparation and thermo-optical characteristics of a smart polymer-stabilized liquid crystal thin film based on smectic A-chiral nematic phase transition. *Smart Materials and Structures*, 23(12):125038, 2014. URL http://stacks.iop.org/0964-1726/23/i=12/a=125038.

[7] Johan Hoogboom, Johannes A.A.W Elemans, Alan E Rowan, Theo H.M Rasing, and Roeland J.M Nolte. The development of self-assembled liquid crystal display alignment layers. *Philosophical Transactions of the Royal Society of London A: Mathematical, Physical and Engineering Sciences*, 365(1855):1553–1576, 2007. ISSN 1364-503X. doi: 10.1098/rsta.2007.2031.

[8] P Dasgupta, M K Das, and B Das. Fast switching negative dielectric anisotropic multicomponent mixtures for vertically aligned liquid crystal displays. *Materials Research Express*, 2(4):045015, 2015. URL http://stacks.iop.org/2053-1591/2/i=4/a=045015.

[9] F. Brochard, L. Léger, and R. B. Meyer. Freedericksz transition of a homeotropic nematic liquid crystal in rotating magnetic fields. *J. Phys. Colloques*, 36(C1):C1–209–C1–213, 1975. doi: 10.1051/jphyscol:1975139.

[10] Ágnes Buka and Nándor Éber, editors. *Flexoelectricity in Liquid Crystals: Theory, Experiments and Applications*. World Scientific, 2012. ISBN 978-1-84816-799-5.

[11] Aayush A. Shah, Heekyoung Kang, Kevin L. Kohlstedt, Kyung Hyun Ahn, Sharon C. Glotzer, Charles W. Monroe, and Michael J. Solomon. Self-assembly: Liquid crystal order in colloidal suspensions of spheroidal particles by direct current electric field assembly (small 10/2012). *Small*, 8(10):1551–1562, 2012. ISSN 1613-6829. doi: 10.1002/smll.201290056.

[12] Wei Zhu, Michael Shelley, and Peter Palffy-Muhoray. Modeling and simulation of liquid-crystal elastomers. *Phys. Rev. E*, 83:051703, May 2011. doi: 10.1103/PhysRevE.83.051703.

[13] Wim H. de Jeu, editor. *Liquid Crystal Elastomers: Materials and Applications*. Advances in Polymer Science. Springer, 2012.

[14] J.S. Biggins, M. Warner, and K. Bhattacharya. Elasticity of polydomain liquid crystal elastomers. *Journal of the Mechanics and Physics of Solids*, 60(4):573 – 590, 2012. ISSN 0022-5096. doi: 10.1016/j.jmps.2012.01.008. URL http://www.sciencedirect.com/science/article/pii/S0022509612000166.

[15] Andraž Rešetič, Jerneja Milavec, Blaž Zupančič, Valentina Domenici, and Boštjan Zalar. Polymer-dispersed liquid crystal elastomers. *Nature Communications*, 7:13140, 2016. doi: 10.1038/ncomms13140.

[16] Joon Heo, Jae-Won Huh, and Tae-Hoon Yoon. Fast-switching initially-transparent liquid crystal light shutter with crossed patterned electrodes. *AIP Advances*, 5(4):047118, 2015. doi: 10.1063/1.4918277.

[17] M. Humar and I. Muševič. 3d microlasers from self-assembled cholesteric liquid-crystal microdroplets. *Opt. Express*, 18(26):26995–27003, Dec 2010. doi: 10.1364/OE.18.026995. URL http://www.opticsexpress.org/abstract.cfm?URI=oe-18-26-26995.

[18] Harry Coles and Stephen Morris. Liquid-crystal lasers. *Nature Photonics*, 4(10):676–685, Oct 2010.

[19] Miguel Camacho-Lopez, Heino Finkelmann, Peter Palffy-Muhoray, and Michael Shelley. Fast liquid-crystal elastomer swims into the dark. *Nature Materials*, 3(5):307–310, May 2004.

[20] Taylor H. Ware, Michael E. McConney, Jeong Jae Wie, Vincent P. Tondiglia, and Timothy J. White. Voxelated liquid crystal elastomers. *Science*, 347(6225):982–984, 2015. doi: 10.1126/science.1261019. URL http://www.sciencemag.org/content/347/6225/982.abstract.

[21] Igor Muševič and Slobodan Žumer. Liquid crystals: Maximizing memory. *Nature Materials*, 10(4):266–268, April 2011.

[22] Teresa Lopez-Leon and Alberto Fernandez-Nieves. Drops and shells of liquid crystal. *Colloid and Polymer Science*, 289(4):345–359, 2011. ISSN 0303-402X. doi: 10.1007/s00396-010-2367-7.

[23] Simon Čopar, Uroš Tkalec, Igor Muševič, and Slobodan Žumer. Knot theory realizations in nematic colloids. *Proceedings of the National Academy of Sciences*, 112(6):1675–1680, 2015. doi: 10.1073/pnas.1417178112. URL http://www.pnas.org/content/112/6/1675.abstract.

[24] Jonathan K. Whitmer, Xiaoguang Wang, Frederic Mondiot, Daniel S. Miller, Nicholas L. Abbott, and Juan J. de Pablo. Nematic-field-driven positioning of particles in liquid crystal droplets. *Phys. Rev. Lett.*, 111:227801, Nov 2013. doi: 10.1103/PhysRevLett.111.227801.

[25] Mingsheng Wang, Le He, Serkan Zorba, and Yadong Yin. Magnetically actuated liquid crystals. *Nano Letters*, 14(7):3966–3971, 2014. doi: 10.1021/nl501302s. URL http://dx.doi.org/10.1021/nl501302s. PMID: 24914876.

[26] Iam-Choon Khoo. *Liquid crystals*, volume 64. John Wiley & Sons, 2007.

[27] Denis Andrienko. Introduction to liquid crystal. *International Max Planck Research School Modelling of soft matter*, 2006.

[28] Iain W Stewart. *The static and dynamic continuum theory of liquid crystals: a mathematical introduction*. CRC Press, 2019.

[29] J.L. Ericksen. Liquid crystals with variable degree of orientation. *Archive for Rational Mechanics and Analysis*, 113(2):97–120, 1991. ISSN 0003-9527. doi: 10.1007/BF00380413.

[30] Iztok Bajc, Frédéric Hecht, and Slobodan Žumer. A mesh adaptivity scheme on the landau-de gennes functional minimization case in 3d, and its driving efficiency. *Journal of Computational Physics*, 321:981 – 996, 2016. ISSN 0021-9991. doi: https://doi.org/10.1016/j.jcp.2016.02.072. URL http://www.sciencedirect.com/science/article/pii/S0021999116001443.

[31] T. Davis and E. Gartland. Finite element analysis of the landau-de gennes minimization problem for liquid crystals. *SIAM Journal on Numerical Analysis*, 35(1):336–362, 1998. doi: 10.1137/S0036142996297448. URL https://doi.org/10.1137/S0036142996297448.

[32] Miha Ravnik and Slobodan Žumer. Landau-degennes modelling of nematic liquid crystal colloids. *Liquid Crystals*, 36(10-11):1201–1214, 2009. doi: 10.1080/02678290903056095. URL https://doi.org/10.1080/02678290903056095.

[33] Sören Bartels and Alexander Raisch. Simulation of q-tensor fields with constant orientational order parameter in the theory of uniaxial nematic liquid crystals. In Michael Griebel, editor, *Singular Phenomena and Scaling in Mathematical Models*, pages 383–412. Springer International Publishing, 2014. ISBN 978-3-319-00785-4. doi: 10.1007/978-3-319-00786-1_17.

[34] Juan-Pablo Borthagaray, Ricardo H. Nochetto, and Shawn W. Walker. A structure-preserving FEM for the uniaxially constrained Q-tensor model of nematic liquid crystals. *Numerische Mathematik*, 145:837 – 881, 2020. doi: 10.1007/s00211-020-01133-z. URL https://doi.org/10.1007/s00211-020-01133-z.

[35] Gi-Dong Lee, James Anderson, and Philip J. Bos. Fast q-tensor method for modeling liquid crystal director configurations with defects. *Applied Physics Letters*, 81(21):3951–3953, 2002. doi: 10.1063/1.1523157. URL https://doi.org/10.1063/1.1523157.

[36] Jia Zhao and Qi Wang. Semi-discrete energy-stable schemes for a tensor-based hydrodynamic model of nematic liquid crystal flows. *Journal of Scientific Computing*, 68 (3):1241–1266, Sep 2016. ISSN 1573-7691. doi: 10.1007/s10915-016-0177-x. URL https://doi.org/10.1007/s10915-016-0177-x.

[37] André M. Sonnet and Epifanio Virga. *Dissipative Ordered Fluids: Theories for Liquid Crystals*. Springer, 2012.

[38] N. J. Mottram and C. J. P. Newton. Introduction to Q-tensor theory. *ArXiv e-prints*, September 2014.

[39] Apala Majumdar. Equilibrium order parameters of nematic liquid crystals in the landau-de gennes theory. *European Journal of Applied Mathematics*, 21(2):181–203, 2010. doi: 10.1017/S0956792509990210.

[40] P. Palffy-muhoray, E. C. Gartland, and J. R. Kelly. A new configurational transition in inhomogeneous nematics. *Liquid Crystals*, 16(4):713–718, 1994. doi: 10.1080/02678299408036543. URL http://dx.doi.org/10.1080/02678299408036543.

[41] A. Sonnet, A. Kilian, and S. Hess. Alignment tensor versus director: Description of defects in nematic liquid crystals. *Phys. Rev. E*, 52:718–722, Jul 1995. doi: 10.1103/PhysRevE.52.718.

[42] X. Lamy. A new light on the breaking of uniaxial symmetry in nematics. *ArXiv e-prints*, July 2013.

[43] M.J. Freiser. Ordered states of a nematic liquid. *Physical Review Letters*, 24(19):1041, 1970.

[44] L.J. Yu and A. Saupe. Observation of a biaxial nematic phase in potassium laurate-1-decanol-water mixtures. *Physical Review Letters*, 45(12):1000, 1980.

[45] Bharat R. Acharya, Andrew Primak, and Satyendra Kumar. Biaxial nematic phase in bent-core thermotropic mesogens. *Phys. Rev. Lett.*, 92:145506, Apr 2004. doi: 10.1103/PhysRevLett.92.145506. URL https://link.aps.org/doi/10.1103/PhysRevLett.92.145506.

[46] L. A. Madsen, T. J. Dingemans, M. Nakata, and E. T. Samulski. Thermotropic biaxial nematic liquid crystals. *Phys. Rev. Lett.*, 92:145505, Apr 2004. doi: 10.1103/PhysRevLett.92.145505. URL https://link.aps.org/doi/10.1103/PhysRevLett.92.145505.

[47] Veena Prasad, Shin-Woong Kang, KA Suresh, Leela Joshi, Qingbing Wang, and Satyendra Kumar. Thermotropic uniaxial and biaxial nematic and smectic phases in bent-core mesogens. *Journal of the American Chemical Society*, 127(49):17224–17227, 2005.

[48] Ricardo H. Nochetto, Shawn W. Walker, and Wujun Zhang. A finite element method for nematic liquid crystals with variable degree of orientation. *SIAM Journal on Numerical Analysis*, 55(3):1357–1386, 2017. doi: 10.1137/15M103844X. URL https://doi.org/10.1137/15M103844X.

[49] Ricardo H. Nochetto, Shawn W. Walker, and Wujun Zhang. Numerics for liquid crystals with variable degree of orientation. In *Symposium NN - Mathematical and Computational Aspects of Materials Science*, volume 1753 of *MRS Proceedings*, 2015. doi: 10.1557/opl.2015.159. URL http://journals.cambridge.org/article_S1946427415001591.

[50] Ricardo H. Nochetto, Shawn W. Walker, and Wujun Zhang. The ericksen model of liquid crystals with colloidal and electric effects. *Journal of Computational Physics*, 352:568 – 601, 2018. ISSN 0021-9991. doi: https://doi.org/10.1016/j.jcp.2017.09.035. URL http://www.sciencedirect.com/science/article/pii/S0021999117306952.

[51] Jia Zhao, Xiaofeng Yang, Jie Shen, and Qi Wang. A decoupled energy stable scheme for a hydrodynamic phase-field model of mixtures of nematic liquid crystals and viscous fluids. *Journal of Computational Physics*, 305:539 – 556, 2016. ISSN 0021-9991. doi: https://doi.org/10.1016/j.jcp.2015.09.044. URL http://www.sciencedirect.com/science/article/pii/S0021999115006439.

[52] Apala Majumdar and Arghir Zarnescu. Landau-de gennes theory of nematic liquid crystals: the oseen-frank limit and beyond. *Archive for rational mechanics and analysis*, 196(1): 227–280, 2010.

[53] Luc Nguyen and Arghir Zarnescu. Refined approximation for minimizers of a landau-de gennes energy functional. *Calculus of Variations and Partial Differential Equations*, 47 (1-2):383–432, 2013.

[54] Jorge Nocedal and Stephen J. Wright. *Numerical Optimization*. Springer Series in Operations Research. Springer, 2nd edition, 2006.

[55] Gianni Dal Maso, Marco Forti, Mario Miranda, Sergio A. Spagnolo, and Luigi Ambrosio, editors. *Selected Papers*. Springer Collected Works in Mathematics. Ennio De Giorgi, 2006. ISBN 978-3-642-40379-8.

[56] B. T. Polyak. Some methods of speeding up the convergence of iteration methods. *USSR Computational Mathematics and Mathematical Physics*, 4(5):1 – 17, 1964. ISSN 0041-5553. doi: https://doi.org/10.1016/0041-5553(64)90137-5. URL http://www.sciencedirect.com/science/article/pii/0041555364901375.

[57] Yurii E. Nesterov. A method of solving a convex programming problem with convergence rate $o(1/k^2)$. *Dokl. Akad. Nauk SSSR*, 269:543–547, 1983.

[58] S. M. Wise, C. Wang, and J. S. Lowengrub. An energy-stable and convergent finite-difference scheme for the phase field crystal equation. *SIAM J. Numer. Anal.*, 47(3):2269–2288, June 2009. ISSN 0036-1429. doi: 10.1137/080738143.

[59] J. Shen and X. Yang. Numerical approximations of Allen-Cahn and Cahn-Hilliard equations. *Discrete Contin. Dyn. Syst.*, 28(4):1669 – 1691, 2010.

[60] J. Shen and X. Yang. A phase-field model and its numerical approximation for two-phase incompressible flows with different densities and viscosities. *SIAM Journal of Scientific Computing*, 32(3):1159–1179, 2010.

[61] Shawn W. Walker. FELICITY: A Matlab/C++ toolbox for developing finite element methods and simulation modeling. *SIAM Journal on Scientific Computing*, 40(2):C234–C257, 2018. doi: 10.1137/17M1128745. URL `https://doi.org/10.1137/17M1128745`.

[62] Artem Napov and Yvan Notay. An algebraic multigrid method with guaranteed convergence rate. *SIAM Journal on Scientific Computing*, 34(2):A1079–A1109, 2012. doi: 10.1137/100818509.

[63] Artem Napov and Yvan Notay. Algebraic analysis of aggregation-based multigrid. *Numerical Linear Algebra with Applications*, 18(3):539–564, 2011. ISSN 1099-1506. doi: 10.1002/nla.741.

VITA

Edison Chukwuemeka grew up in Lagos, Nigeria and obtained his Bachelors' degree in Mechanical Engineering from the University of Lagos, Akoka in Fall of 2008. After graduation, he worked with Schlumberger Nigeria for 3.5 years before enrolling to graduate school. Currently, he is a candidate for Maters degree in Applied Mathematics to be awarded in May 2021.